TURUN YLIOPISTO

Accuracy and precision comparison with elemental analysis parameter optimization for XRF, OES, and SEM-EDS

Materials Engineering/Faculty of Technology
Master's thesis
Department of Mechanical and Materials Engineering

Author:
Matias Kallio

05.02.2025
Turku

Master's thesis

Subject: Materials Engineering
Author: Matias Kallio
Title: Accuracy and precision comparison with elemental analysis parameter optimization for XRF, OES, and SEM-EDS
Supervisors: Dr. Emilia Palo (UTU) and MSc(tech) Markus Aarniluoma (Wärtsilä)
Number of pages: 65 pages
Date: 05.02.2025

Scanning Electron Microscope (SEM) with Energy Dispersive Spectrometer (EDS) is a widely used technique in various industries and applications due to its ability to image nanoscale structures with high resolution. EDS enhances the use of SEM as it produces qualitative and quantitative information based on characteristic X-rays emitted from the sample. Optical Emission Spectroscopy (OES) and X-ray fluorescence (XRF) are mature techniques for high-quality and fast elemental analysis with quick sample preparation.

This thesis investigates the accuracy and precision of elemental analysis techniques, including SEM-EDS, OES, and XRF. Experimental analysis also focuses on different surface qualities, such as cones, grooves or fracture surface and aims to determine the optimal parameters in elemental analysis for each technique. Furthermore, the purpose is to explore the effects of different surface qualities and determine the optimal parameters in that scope that is possible in these circumstances.

Results obtained in this study indicate the superior performance of OES in quantitative elemental analysis for both major and trace elements, highlighting the SEM-EDS capabilities for examining specially shaped samples, such as cones, grooves, and fracture surfaces. XRF exceeded the performance of EDS in quantitative analysis and precision, but limitations occurred with light elements ($Z < 11$) and accuracy. Overall, the study gives detailed insights into characterization and operation of different elemental analysis techniques highlighting the importance of sample preparation and correct operational parameters.

Keywords: Chemical analysis, Scanning Electron Microscope, Energy Dispersive Spectroscopy, Optical Emission Spectroscopy, X-ray fluorescence, Accuracy, Precision

Diplomityö

Oppiaine: Materiaalitekniikka
Tekijä: Matias Kallio
Otsikko: Accuracy and precision comparison with elemental analysis parameter optimization for XRF, OES, and SEM-EDS
Ohjaajat: FT Emilia Palo (UTU) ja DI Markus Aarniluoma (Wärtsilä)
Sivumäärä: 65 sivua
Päivämäärä: 05.02.2025

Pyyhkäisyelektronimikroskooppi (SEM) yhdessä energiadispersiivisen spektroskopian (EDS) kanssa on laajasti käytetty menetelmä eri teollisuudenaloilla ja sovelluksissa, sillä se mahdollistaa nanomittakaavan rakenteiden kuvantamisen korkealla resoluutiolla. EDS tehostaa SEM:n käyttöä tuottamalla kvalitatiivista ja kvantitatiivista informaatiota näytteestä emittoituvien karakterististen röntgensäteiden perusteella. Optinen emissiospektroskopia (OES) ja röntgenfluoresenssi (XRF) ovat vakiintuneita menetelmiä nopeaan ja korkealaatuiseen alkuaineanalyysiin, jossa myös näytteiden valmistus on nopeaa ja yksinkertaista.

Tämä diplomityö tutkii yllä mainittujen alkuaineanalyysitekniikoiden (SEM-EDS, OES, XRF) mittaustarkkuutta ja toistettavuutta. Kokeellisessa analyysissä tutkitaan myös erilaisten pinnanlaatujen, kuten kuoppien, urien ja murtopintojen vaikutusta, ja pyritään määrittämään optimaaliset parametrit kullekin menetelmälle niin tarkasti kuin se näissä olosuhteissa on mahdollista.

Tutkimuksen tulokset osoittavat, että OES on ylivoimainen menetelmä kvantitatiiviseen alkuaineanalyysiin sekä pienillä että suurilla pitoisuuksilla. SEM-EDS puolestaan soveltuu erityisesti monimuotoisten näytteiden, kuten kuoppien, urien ja murtopintojen tutkimiseen. XRF ylitti EDS:n suorituskyvyn kvantitatiivisessa alkuaineanalyysissä ja toistettavuudessa, mutta sen tarkkuudessa ja kevyiden alkuaineiden ($Z < 11$) havaitsemisessa esiintyi rajoitteita. Kokonaisuudessaan tutkimus tarjoaa yksityiskohtaista tietoa eri alkuaineanalyysitekniikoiden karakterisoinnista ja toiminnasta, korostaen näytteenvalmistuksen ja huolella valittujen parametrien merkitystä.

Avainsanat: Alkuaineanalyysi, pyyhkäisyelektronimikroskooppi, energiadispersiivinen spektroskopia, optinen emissiospektroskopia, röntgenfluoresenssi, mittaustarkkuus, optimointi

Acknowledgments

I am grateful to MSc(tech) and Senior Technical Expert Markus Aarniluoma from Wärtsilä for inducting me into the use of chemical analysis techniques and sample preparation methods. He gave a detailed introduction which included theoretical and experimental training for each analytical technique before starting the actual work. I also extend my gratitude to Senior Technical Support Engineer Sami Saarela who was responsible for cutting the samples from different components and assisting with the sample preparation. The overall investigation team was very supportive and easy to adapt, and I always had the feeling that if I had some open questions, I could ask with a low threshold. Furthermore, I express my appreciation to Dr. Emilia Palo from University of Turku, for her support and advice related to thesis structure, small details, and writing tips during the whole thesis process.

Table of contents

Nomenclature

Abbreviation	Explanation
BI	Beam intensity
BSE	Back-scattered electron
DT	Destructive testing
EDS	Energy dispersive spectroscopy
EMI	Electromagnetic interference
ICR	Input count rate
LOD	Limit of detection
LOQ	Limit of quantification
NDT	Non-destructive testing
OCR	Output count rate
OES	Optical emission spectroscopy
RE	Relative error
RSD	Relative standard deviation
SDD	Silicon drift detector
SD	Standard deviation
SE	Secondary electron
SEM	Scanning electron microscope
WD	Working distance
WDS	Wavelength dispersive spectroscopy
XRF	X-ray fluorescence

1 Introduction

Failure analysis has a significant role in various industries, especially in the automotive, marine, and aerospace industries. It is used to investigate the root cause of component failure to prevent such situations in the future and possibly enhance the used materials. Individual elements in an alloy can either improve its properties or cause undesirable effects [1]. A major part of the analysis is the use of different analytical techniques, which can include destructive (DT) or non-destructive (NDT) testing and chemical analysis, which can be performed using wet chemistry or instrumental methods [2]. The range of methods for quantitative analysis of metal alloys is wide as the materials, failure types and shapes and even the investigators are different. The selection of suitable analytical techniques depends on the required chemical information, the condition of the sample, and any restrictions set by stakeholders [1].

Analytical techniques that are applicable for failure analysis in various industrial sectors have developed continuously in recent decades and the trend has intensified in recent years [3]. Scanning electron microscope (SEM) with energy dispersive spectroscopy (EDS) is an extensively used technique for elemental analysis in many applications [4]. SEM is also the most widely used technique for analyzing failed components in both oil and gas industry as in the marine structure investigations [3, 5]. EDS is primarily used for qualitative material analysis but it can also be used to produce semi-quantitative results [3]. Furthermore, the contemporary use of SEM and EDS in cases where spot analysis is needed is highly advantageous [3].

Optical emission spectroscopy (OES) is one of the most popular methods for chemical analysis and metal alloy identification. The most used technique for bulk analysis of metal alloys is spark-emission OES, which is also widely used in failure analysis both qualitative and quantitative determination of major and trace elements in metal alloys [1]. Techniques can be further divided into glow discharge (GD-OES) and inductively coupled plasma (ICP-OES) [1]. It has certain benefits such as speed, price, and quick sample preparation that make it useful for a wide range of applications and the current trend is principally toward complete automation [6]. X-ray fluorescence (XRF) can be applied to qualitative and quantitative chemical analysis across a wide range of research areas. However, XRF is most advantageous in fast on-site measurements as it cannot match the accuracy of OES, when providing elemental compositions due to higher detection limit {3].

The use of analytical techniques is not efficient if the measurement accuracy, precision, and operational parameters are not familiar. Accuracy and precision are the most important factors that are used to determine the quality of analysis. Accuracy refers the closeness of the measured value to the known true value as the precision determines the repeatability of measurement or method. In addition, sample preparation has a major impact on the results as the smallest impurities can lead to results with high deviation and error. This thesis aims to answer the open questions that are related to the presented analytical techniques SEM-EDS, OES, and XRF.

1.1 Background of the thesis

The idea for this thesis became topical as there was interest to enhance the use of analytical techniques in Wärtsilä Turku Investigation Laboratory (TIL). A wide-range comparative review was needed to investigate the most accurate and precise device for certain purposes of use as the investigated samples include different materials and different shapes (cones and grooves) or surfaces (fractured or corroded). The OES has been the most accurate device for elemental analysis according to investigators in Wärtsilä but there has also occurred a phenomenon which is unknown but has a significant impact on the analysis. Furthermore, the efficient use of measurement parameters is another part of the enhancement of the total analysis process.

The main purpose of this thesis is to make the usage of the mentioned analytical devices more understandable and clearer and to increase the knowledge related to parameters and measurement inaccuracy in chemical analysis. Generally, only a few previous studies were done that are related to the comparison of this kind of analytical techniques [7]. Figure 1 illustrates the trend of publications that are related to keywords SEM, EDS, XRF in a same study which has grown evenly from 2010 to 2024. However, when adding OES to the keywords there came no search results which indicates that this kind of analytical technique comparison is relatively rare among these presented techniques. From that perspective, it is more meaningful to perform this kind of analytical comparison.

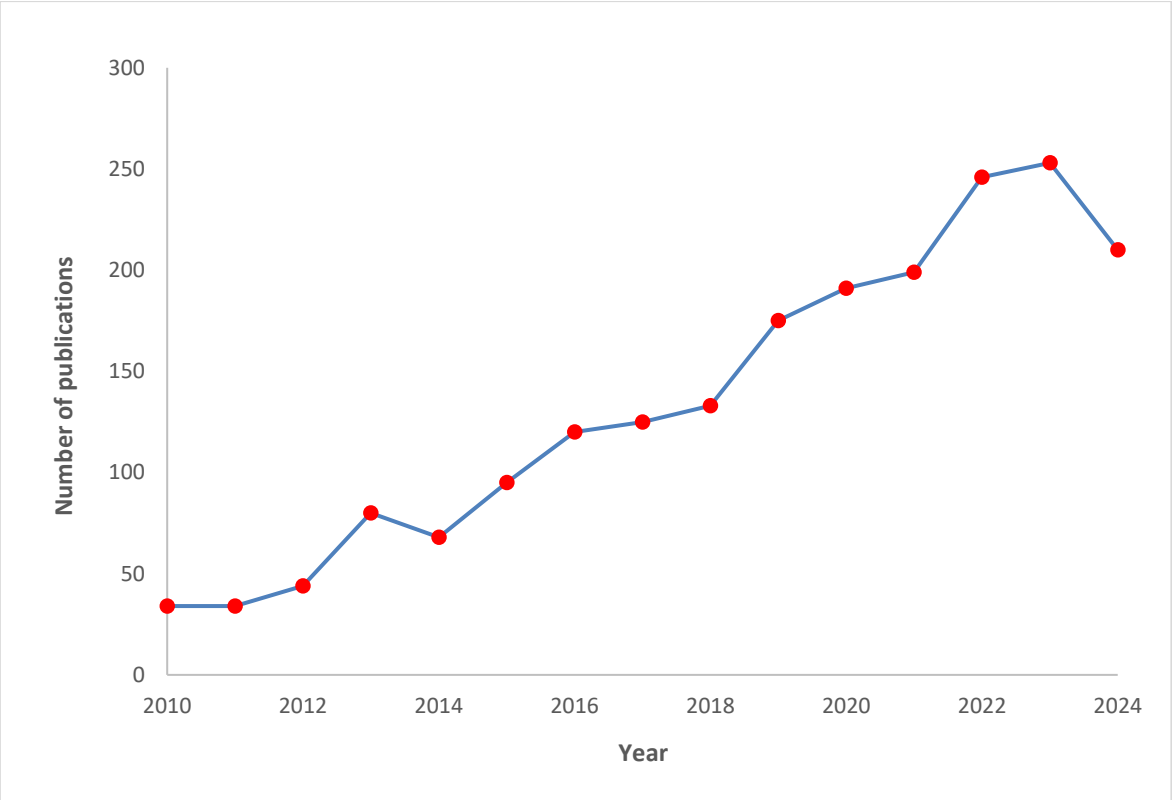

Figure 1. The publication chart of articles searched from the Scopus database with the keywords "SEM", "EDS" and "XRF".

1.2 Aim and research questions

The main purpose of this study is to investigate the measurement accuracy and precision of XRF, OES, and SEM-EDS. Another important aspect is to research the effect of different surface qualities. In addition, the parameter optimization is performed as deeply as possible under these circumstances. This is done by answering the following research questions:

- How to avoid carbon fluctuation in measurement results? (OES)
- Are the chemical composition results from light elements reliable? (EDS, XRF)
- How to optimize operational parameters? (EDS, OES, XRF)
- How does the surface quality (cones, grooves, fractures, and rust) affect the measurement results? (EDS)
- What is the most precise and accurate device for elemental analysis? (EDS, OES, XRF)

2 Introduction to the analytical techniques

Analytical techniques in this study, which are X-ray fluorescence (XRF), scanning electron microscope with energy dispersive spectroscopy (SEM-EDS), and optical emission spectroscopy (OES) can be separated according to the emission source: X-ray, electron, and optical light (wavelength) based techniques. XRF can be further divided into different categories, as shown in Figure 2. Different electron excitation-based techniques are categorized in Figure 4 in section 2.2. In addition, optical emission spectrometers can be divided into spark OES, GD-OES, and ICP-OES. The basic physics of X-ray generation and interactions between the specimen and various emission sources are presented at a general level as the focus is on the operating principles, parameters, and applications of the analytical techniques.

2.1 X-ray fluorescence techniques

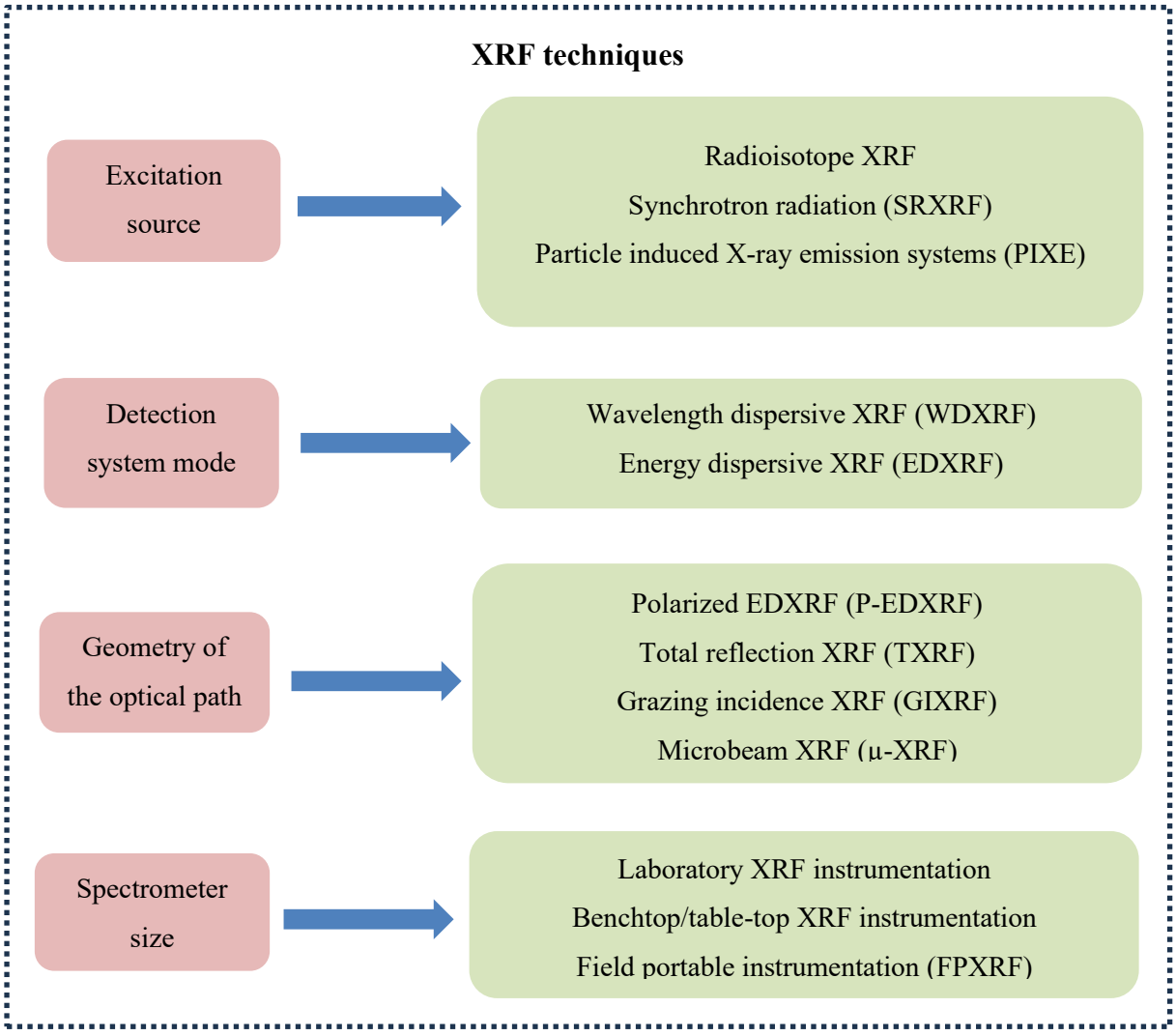

Figure 2. Classification of different XRF techniques and related techniques. Image reproduced and modified from [8].

X-ray fluorescence (XRF) is a non-destructive technique to analyze and determine the elemental composition of materials. XRF detects and analyses the characteristic X-rays emitted from the specimen after it is excited by high-energy primary X-rays [9]. The incoming X-rays are differentiated with an analytical crystal which diffracts the radiation to different extents according to Bragg's law (Formula 1) [10]. The structure of an XRF instrument consists of the following parts: the X-ray source that generates the primary X-rays, the specimen presentation system, the detection system, and the data collection and processing system [8]. The most used source is an X-ray tube with tungsten anode to produce 0.5-3 kW of power and 30 – 150 kV of voltage [9, 10]. The structure and components of handheld XRF are presented in Figure 3.

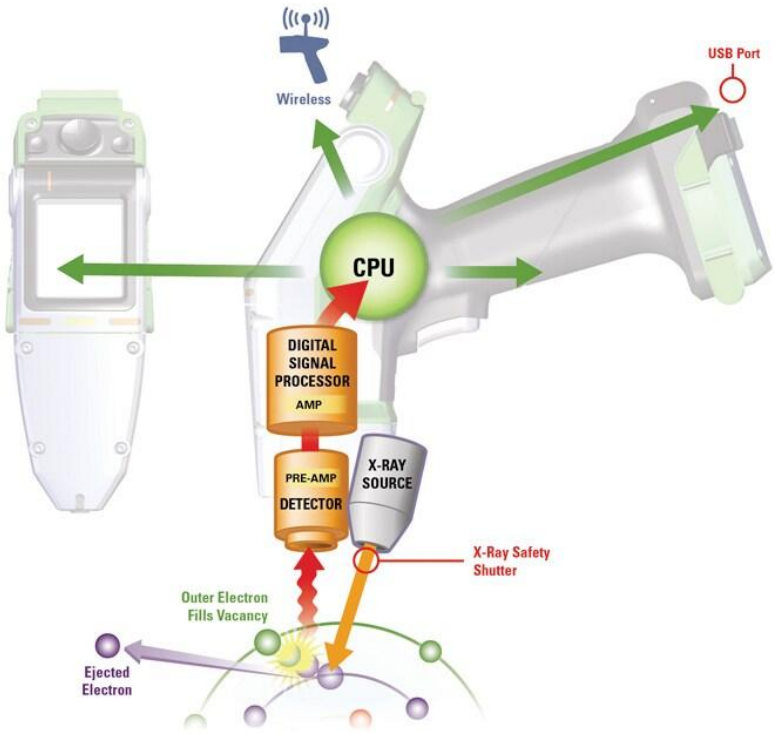

Figure 3. Schematic illustration of the structure of handheld XRF. Image reproduced from [11].

XRF techniques can be divided into wavelength (WDXRF) and energy dispersive (EDXRF) system [8]. Furthermore, the analysis of characteristic X-rays can be done from either their wavelengths or energies. The qualitative and quantitative elemental information of the sample in WDXRF analysis is based on Bragg's law which is as follows:

$$n\lambda = 2d_{hkl} \sin\theta \quad (1)$$

where n is the order of diffraction, λ is the wavelength of X-rays, d_{hkl} is the interplanar spacing and sin θ is the incident and diffraction angle. EDXRF measures the intensity of the characteristic X-ray peaks simultaneously to produce information of the elements and their

amounts in the sample [8]. XRF can be used for both quantitative and qualitative analysis as each of the elements in the sample produces characteristic X-rays but the nature of the information is more quantitative [11, 12]. Measurements can be performed directly from the desired surface, and no big preparations are needed [14]. However, only elements near to the surface are irradiated which makes XRF susceptible to surface contamination and roughness of the sample [1]. X-ray energies have different requirements for surface roughness as the energies above 5 keV prefer roughness of 100 µm, and low energy levels (down to 2 keV) require 20-40 um surface roughness [8]. In theory, XRF can detect the emission of X-rays even from the light elements but in practice, the limitation begins when the atomic number is less than eleven (Na) [15]. The selection of appropriate counting time is crucial as precision usually decreases when increasing the measurement time [8].

2.2 Electron microscopy techniques

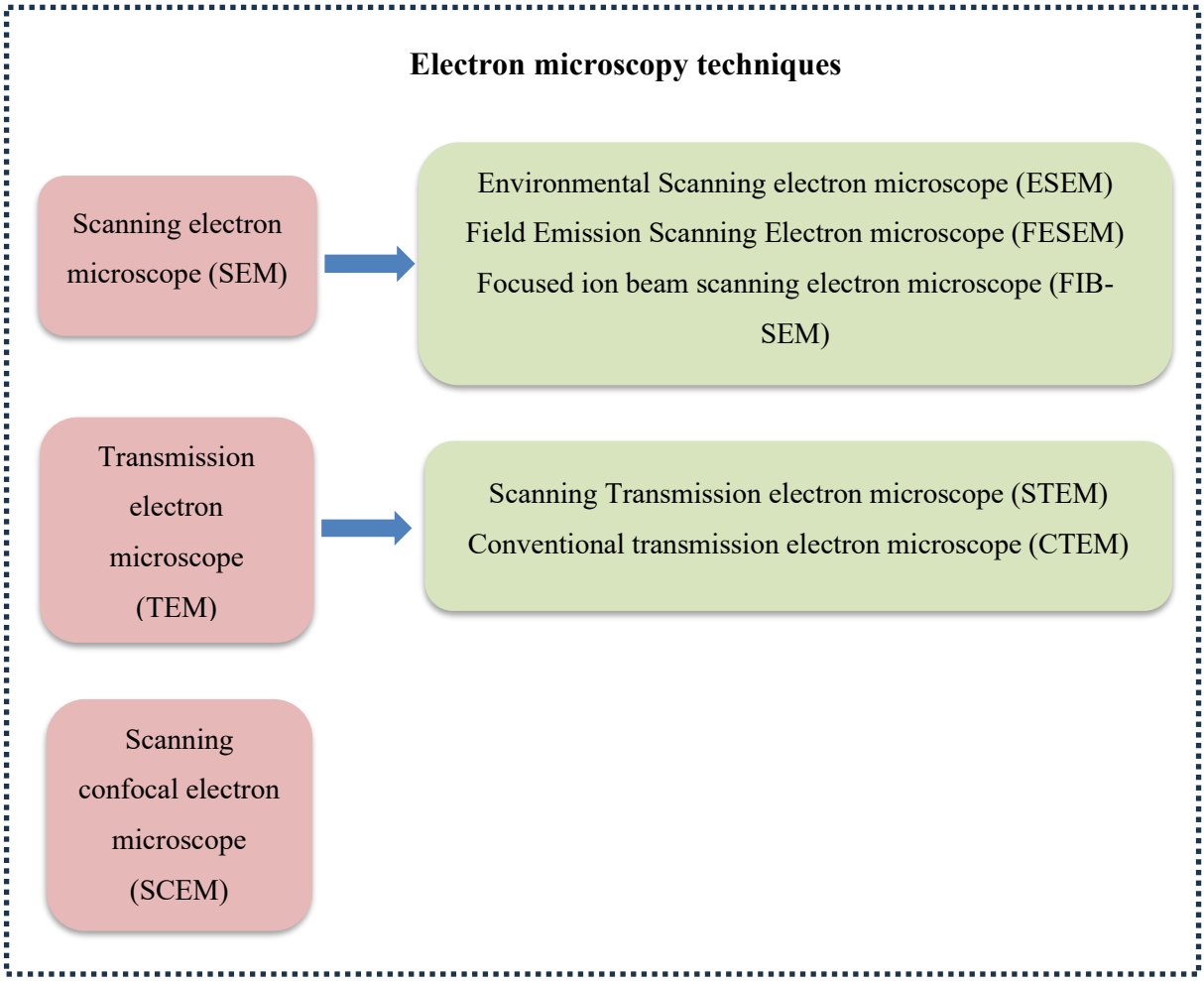

Figure 4. Classification of different electron excitation-based microscopy techniques.

Scanning electron microscopy is the most widely used technique in the context of electron microscopes. Other related electron microscopy techniques are presented in Figure 4. SEM is also the most common technique for failure analysis in oil, gas, and marine industries and if equipped with an EDS detector it can detect and quantify almost every element present in the periodic table except H, He, and Li [3, 4]. SEM is used to observe the microscopic structures of the sample by scanning the surface with a high resolution and high depth of field, which provides the possibility of generating a three-dimensional image. The image is formed with a focused ion beam which scans the whole surface area of the specimen [9]. Even the failure modes can be identified through morphological features obtained from the fracture surface analysis [3]. Furthermore, the use of SEM can be enhanced with a various additional detectors (EDS or WDS) which are presented more specifically in chapter 2.4. SEM structure consists of high energy electron gun, various magnetic lenses, and apertures. SEM structure and operating principle are presented more specifically in Figure 5.

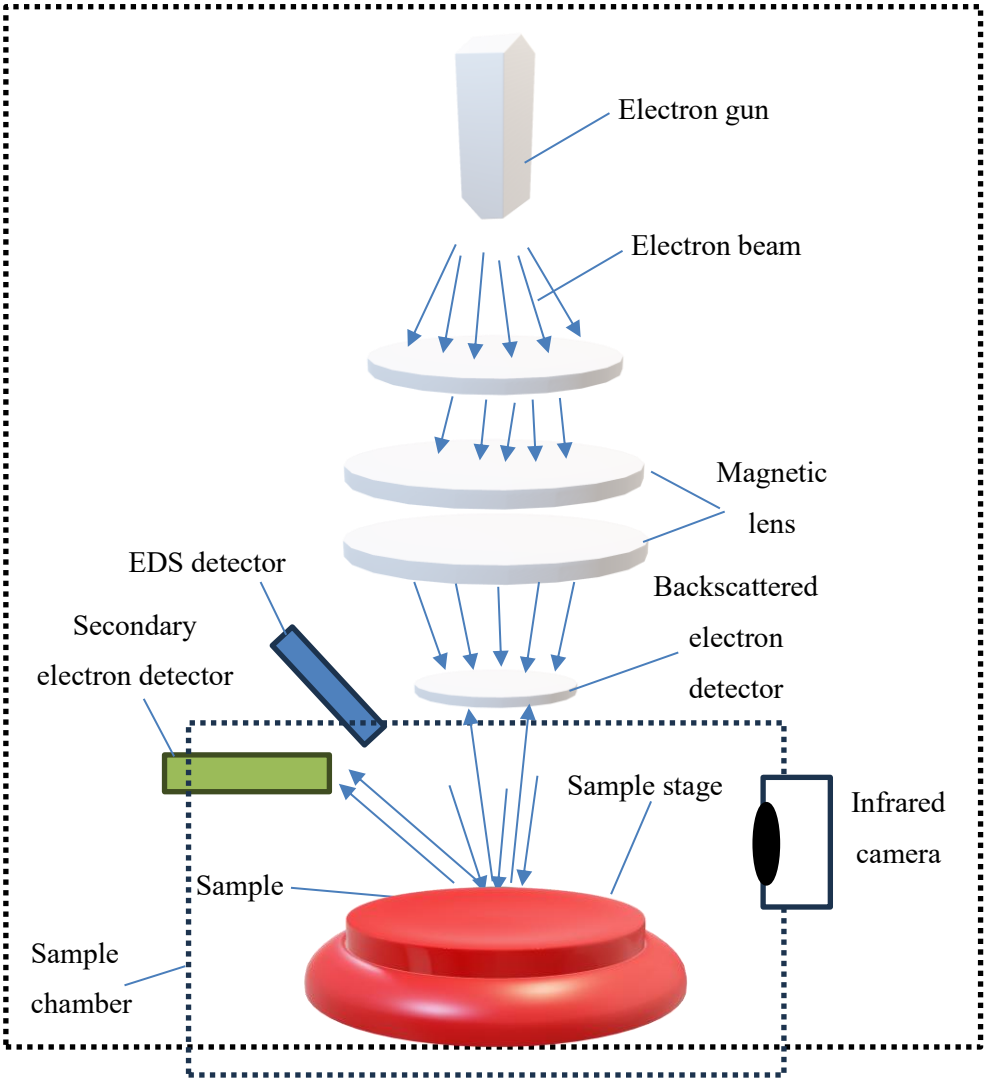

Figure 5. Schematic illustration of SEM-EDS structure and operating principle.

SEM operating conditions and parameters are crucial in materials science, particularly the accelerating voltage. It is the voltage that is applied to the filament and in accordance with a small current, it forces the electrons out of the filament and makes them penetrate the material [16]. Penetration depth is dependent on the atomic number, beam energy, and specimen tilt. Low accelerating voltage produces small beam penetration and more information about the surface structure. On the other hand, high accelerating voltage creates more information of the internal structure resulting in losses in fine details of the surface. The voltage used (kV) has also impacts on area measurements as Yanez et al. studied the changes in particle area measurements for metallic and polymeric materials with different accelerating voltages and magnification [17].

The selection of the correct accelerating voltage is also critical for proper X-ray generation. Correct voltage is dependent on the elements present in the sample and the energy of electrons in the primary beam (E_0) must be higher than the critical ionization energy [18]. The ratio of these two energies is called overvoltage ratio (E_0/E_C) and it should be over 2 [18]. The importance of correct accelerating voltage is illustrated in Figure 6.

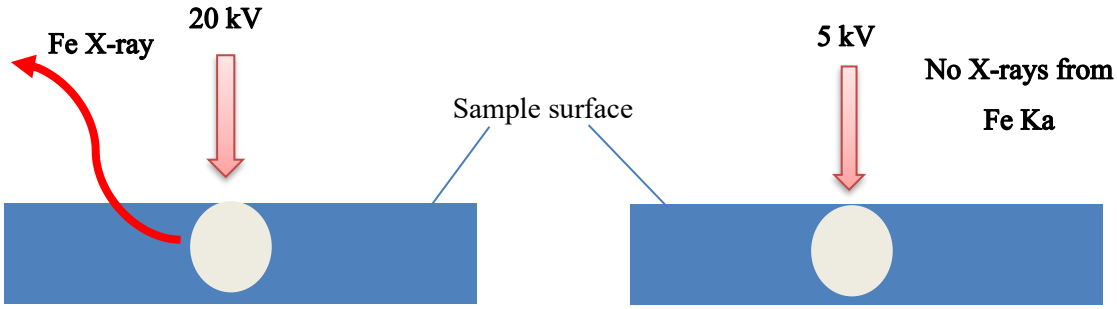

Figure 6. Schematic illustration of the importance of correct accelerating voltage in SEM to produce characteristic X-rays. If the accelerating voltage is too low (lower than the energy levels of detected elements), the characteristic X-rays are not produced.

Non-conductive impurities are visibly brighter in the SEM image compared to other spots that are conductive metal. This phenomenon is called charging effect which occurs when non-conductive specimens are imaged in a high vacuum [9]. The charging effect is caused by the lack of a ground path, which the insulator does not provide [19]. According to Cazaux et al. the charging is minimized if the incident beam energy E_0 is equal to the critical ionization energy E_C [20]. Other common errors that result from charging are image distortion and artifacts [9]. Imaging artifacts in SEM can be divided into three different types: random, time-dependent distortion (scan line shift), non-random, time-independent distortion (spatial distortion), and non-random time-dependent distortion (drift distortion) [21]. These can be reduced with the

optimization of SEM scanning parameters which can include faster scanning, lower beam voltage, and smaller spot size [21].

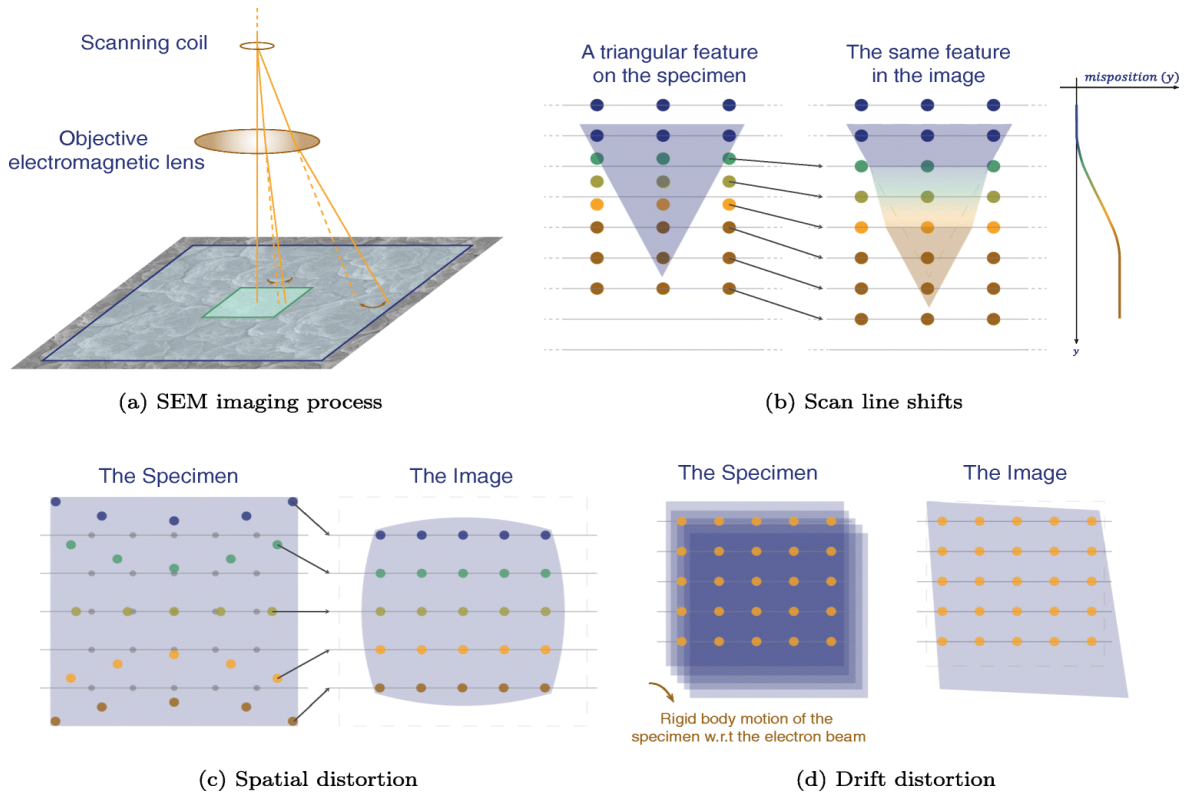

Figure 7. Different imaging artifacts in SEM imaging (a) include scan line shift (b), spatial distortion (c), and drift distortion (d). Image reproduced from Maraghechi et al. [21]. Copyright 2019 Maraghechi et al, published by Springer Nature.

2.3 Interaction signals between specimen and excitation source

Many different signals are generated when the specimen is bombarded with high energy electron beam: secondary, backscattered, elastically scattered, low-loss and Auger electrons, characteristic and continuum X-rays [22]. The most widely used signal for imaging in SEM is a secondary electron as it provides topographical images of the surface [17]. Characteristic X-rays are the primary signals that are used for elemental analysis in EDS. In Figure 8, the characteristic X-ray generation is presented happening in XRF and SEM as they are the two main techniques in this study.

In scanning electron microscope characteristic X-rays are produced by the energy of an electron beam which requires a high vacuum to avoid energy losses of the electron. The energy of the electron beam must be higher than the critical ionization energy E_C for the specific atom and atomic shell(s) [23]. Efficient excitation requires at least two times higher incident beam energy than the critical excitation energy ($E_0 > 2\ E_C$) [24]. In X-ray fluorescence, the atoms of the

material are excited by the X-ray beam, which produces high-energy primary X-rays. After this, the characteristic X-rays are produced in the same way as using the electron beam. The process of generating characteristic X-rays is illustrated for a silicon atom in Figure 8 according to [25].

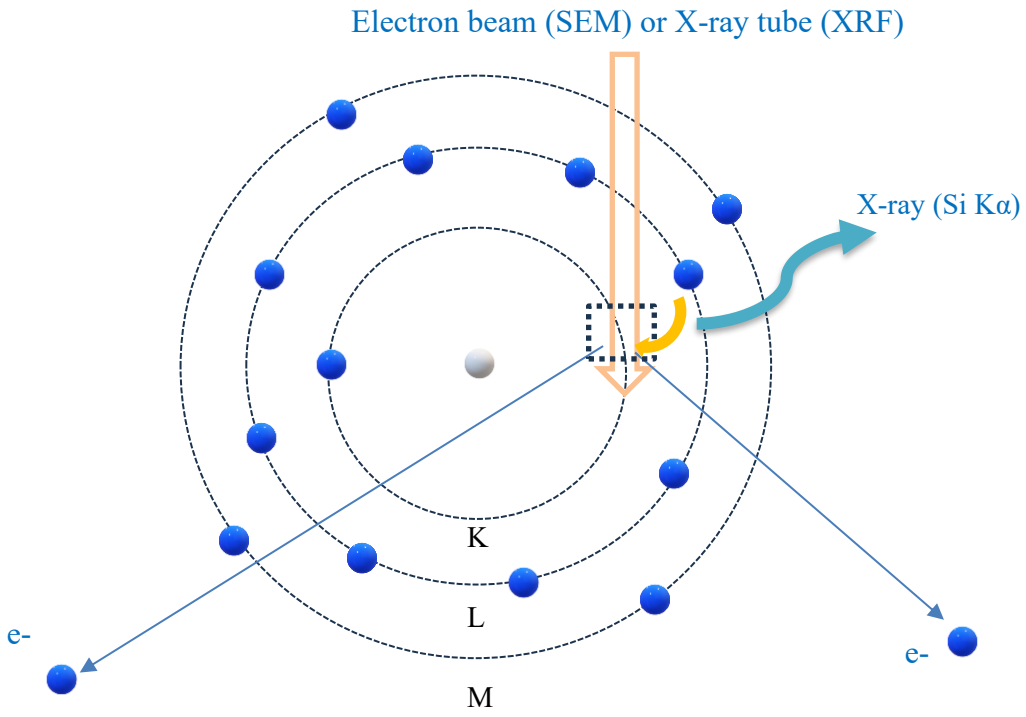

Figure 8. Schematic illustration of characteristic X-ray production in Si atom.

Bremsstrahlung is the other X-ray type which is produced by the interaction of the electron beam and the sample in SEM. These X-rays are commonly indicated as background or continuum X-rays. The production method is related to decelerating primary beam electrons by the electric field which is generated by the atomic nuclei within the sample [23]. Bremsstrahlung X-rays cannot exceed the energy of the incident beam energy (E_0) which makes an upper limit for the X-ray spectrum [26]. If the energy is equal to E_0, the intensity of the X-ray is zero, which is called the Duane-hunt limit (Figure 9). Most of the produced continuum X-rays are low energy (grey area in Figure 9) and the intensity grows significantly below E_0.

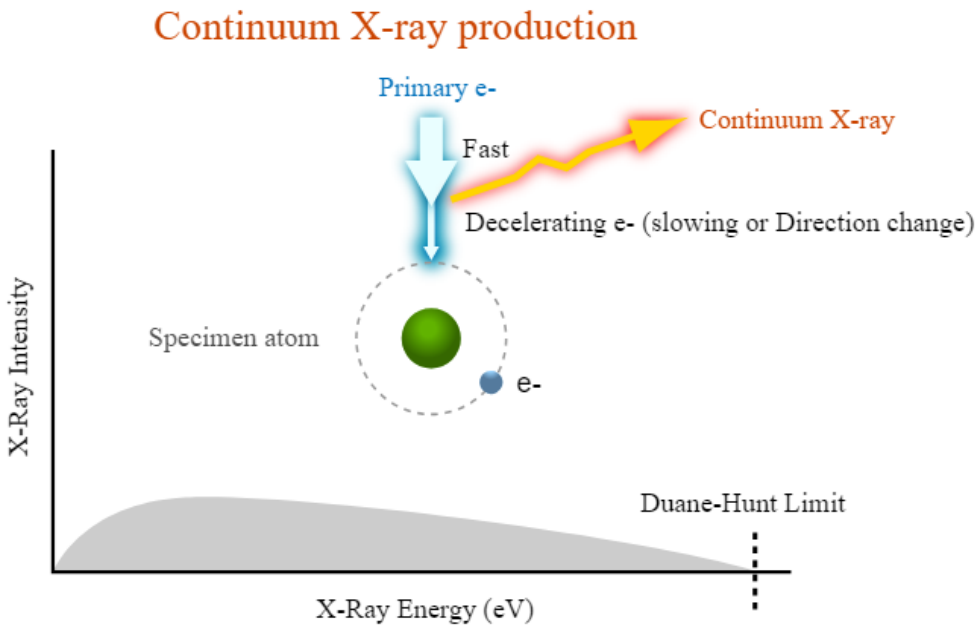

Figure 9. Continuum X-ray production and Duane-Hunt limit illustration. Image is reproduced from [26].

Secondary electrons (low energy) are produced when inelastic scattering of the beam electrons ejects weakly bound valence electrons or conduction band electrons, which have binding energies of 1-15 eV [27]. The most important characteristic of SE is its extremely low kinetic energy. The escape zone of secondary electrons is limited near the specimen surface at a depth of 5-50 nm (Figure 10). SEs are primarily used to generate topographic contrast [22].

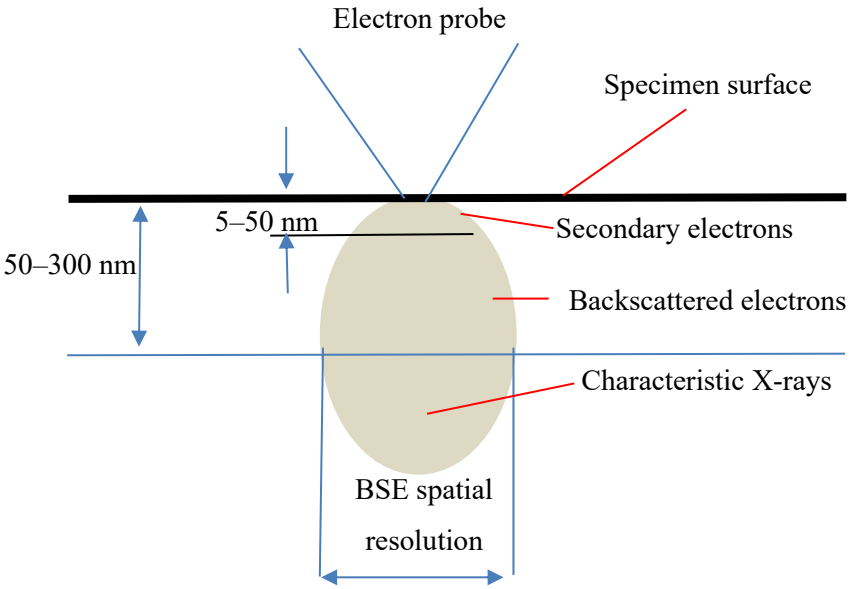

Figure 10. Illustration of the interaction products between the electron beam and sample.

Backscattered electrons (high energy) are produced by the elastic scattering, and they have energy higher than 50 eV [22]. BSEs are used to produce images that provide information about the average atomic number of the sample (atomic-number contrast). The average atomic number is directly proportional to the amount of scattered primary electrons which leads to brighter images of those materials [9]. The resolution of BSE is reduced compared to SE, which is due to deeper penetration of BSEs in the sample [28].

2.4 Energy dispersive spectroscopy (EDS)

EDS is typically included as a part of a scanning electron microscope, which allows the possibility of elemental analysis while studying the microstructure of materials. The detector uses the characteristic X-rays produced by the interaction between the sample and high-energy electron beam to display the X-ray signal as a spectrum of intensity (X-ray count rate) versus energy [9]. This spectrum produces qualitative information, which is the energy of X-rays, and quantitative information, which refers to the intensity of X-ray peaks [29]. EDS creates electrical pulses that are processed and counted with electronic circuitry, which includes a set of amplifiers, various signal processing functions, and a computer for data output [10]. The structure of EDS is graphically illustrated in Figure 11.

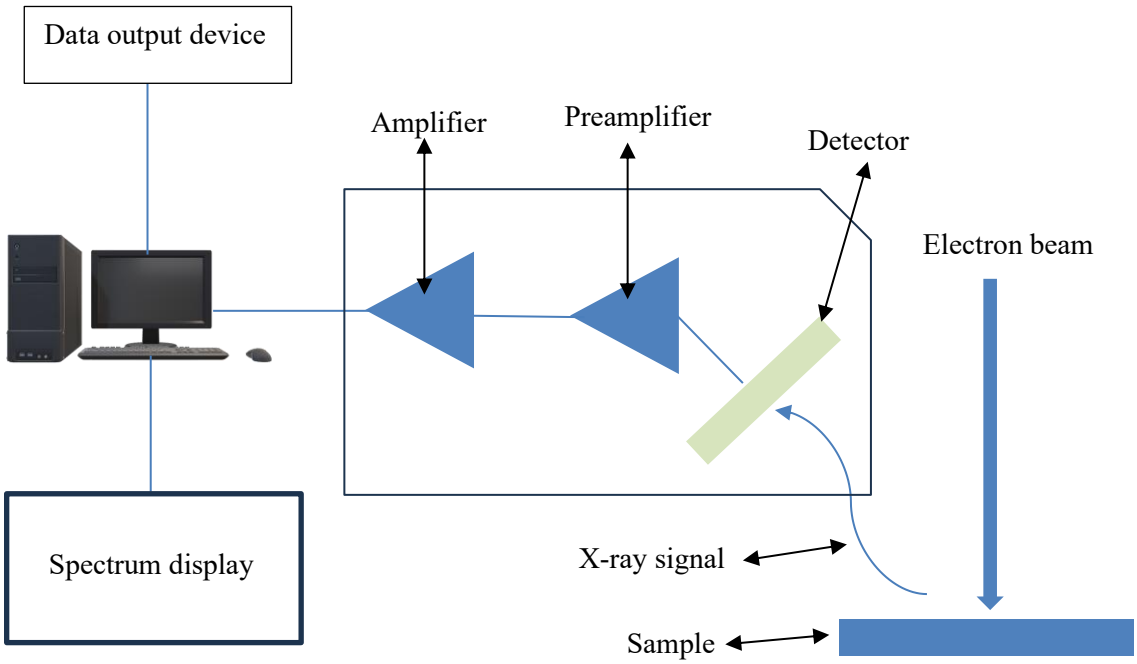

Figure 11. Schematic of the main structure of EDS system together with scanning electron microscope.

The homogeneity of the samples and the surface smoothness are essential to ensure accurate results, especially in EDS analysis [30]. In addition, quantitative analysis with EDS requires separate standard samples that contain the elements in the specimen to be investigated [9]. Elemental analysis in EDS is related to a few parameters: dead time, input count rate (ICR), and output count rate (OCR). Dead time means the percentage of unprocessed X-rays and it can be calculated as follows:

$$Dead\ time = \left(1 - \frac{OCR}{ICR}\right) * 100 \quad (2)$$

Where OCR is the output count rate and ICR is the input count rate. Dead time can be adjusted with beam current as an increase in current increases the dead time [4]. The dead time is usually maintained at 10-20 % if the goal is to perform elemental analysis but it can be even near 50 % [24]. Input count rate refers to the total number of X-rays hitting the detector. This rate can be adjusted with longer acquisition time, higher beam current, or higher accelerating voltage. The output count rate is the number of processed X-rays, which can be calculated using the dead time. The most important value for an analyst is OCR as it covers the X-rays that are processed [31].

Elements with major concentration (> 10 wt%) have the highest peaks in the X-ray spectrum even though peak intensities are not directly proportional to concentration. Other peaks are produced by the minor (1-10 wt%) or trace amount (< 1 wt%) elements. Automated peak identification has been shown to cause infrequent errors even with elements with major concentrations (highest relative intensity peaks). However, this drawback is most problematic at minor (1-10 wt%) and trace (< 1 wt%) levels. The effect of misidentification in these low-concentration levels may seem to be less important compared to major constituents but often those elements have a critical impact on the strength of the material or they act as an analytical fingerprint. [32, 17]

Spectral overlapping is another drawback for element identification as it falsifies the results when close energy peaks, for example, molybdenum L-series (2,31 keV) and sulphur K-series (2,29 keV) cannot be separated from each other. This often leads to a situation where the EDS detector resolution is not high enough to solve overlapping peaks as the spectral resolution is typically from 125 eV to 150 eV, depending on the spectrometer [33]. One option to resolve this drawback is to use a WDS detector which can have a resolution from 50 eV down to 2 eV, which is significantly better than EDS [34]. The detection limit is another parameter in which

WDS performs better than EDS. The detection limit depends on the surface quality as a smoother surface lowers the detection limit [3]. The difference in the close spectral peak handling of EDS and WDS is illustrated in Figure 12.

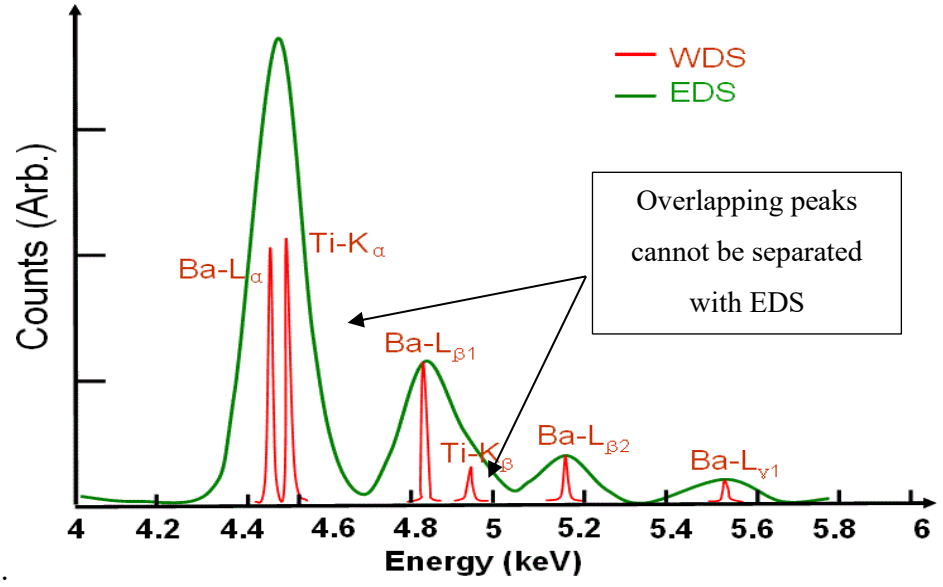

Figure 12. Close spectral peak handling in $BaTiO_3$ with EDS and WDS. Red peaks (WDS) are clearly separated as the green peaks (EDS) are wider and smoother which makes the separation complicated. The image is reproduced and modified from [35].

EDS detectors have achieved technical progress such as digital pulse processing, optimized fast discriminators, and improved algorithms but they are still inferior to WDS spectrometers in quantitative analysis. Above all, the most significant improvement in EDS detectors has been the silicon drift detector (SDD). EDS system has been traditionally equipped with lithium drifted silicon Si (Li) detector, but SDD has provided better resolution and at least ten times better throughput [36]. SDD collects the full spectrum of elements providing both informative and less informative data. Ritchie et al. compared the SDD and WDS which showed that SDD can produce as accurate and precise results than WDS with equivalent or less time and effort [36]. Furthermore, Ritchie et al. concluded that collecting major and minor elements with SDD and leaving the trace elements for WDS reduce time and the need for different spectrometers [36].

2.5 Optical emission spectroscopy

Optical emission spectroscopy (OES) covered in this section refers to spark-induced OES. It is one of the most popular methods for both qualitative and quantitative chemical analysis and metal alloy identification. Other alternative OES methods include GD-OES and ICP-OES. The

main difference between these techniques compared to EDS and XRF is the excitation source and the type of emission that is detected.

Chemical analysis and element identification in OES is based on the unique wavelengths of certain elements [37]. The system is simple as it contains the chamber, spark stand, electrode, and inert gas (commonly Argon) as illustrated in Figure 13. The main component is the spark electrode, which creates an electrical discharge and heats the sample to the ablation point (Figure 13). The electrode acts as an anode and the sample forms as a cathode, which limits the measurement to conductive samples. Electrodes are usually made from tungsten, copper, or silver alloys [38]. An optical device is used to capture the incoming light and separate it into spectral lines (element-specific wavelengths). OES includes the visible spectrum and part of the ultraviolet spectrum, from 130 to 800 nm [24]. Sorting of these wavelengths is done with diffraction grating, which is a reflective surface with a specific shape and parallel grooves that are aligned closely [37]. The intensity of these spectral lines is then measured with the detector. Peak intensities are compared to the peak wavelengths to identify the elements and their quantities in the sample [37].

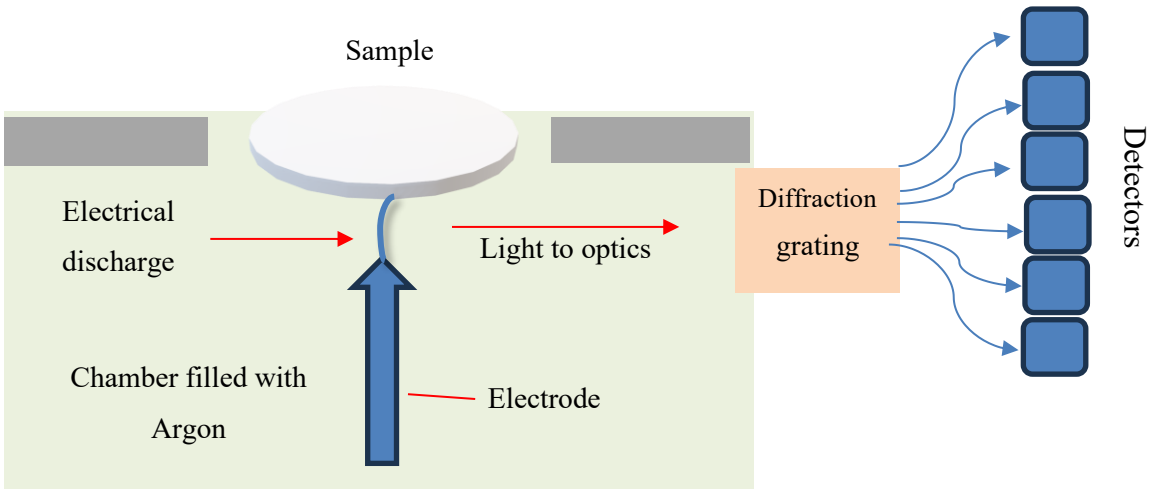

Figure 13. Schematic illustration of OES operating principle. Electrical discharge is generated between the sample and electrode after which the emitted light travels to diffraction grating and for the detection.

OES has certain benefits in measurement speed and sample preparation that make it useful for a wide range of applications. Measurements can be taken fast (from 30 s to several hours) as the sparking process is automated and it can be operated with a computer [6]. Sample preparation can be handled with a grinding machine with different surface qualities as the mesh number of the grinding plate can be in a range of 40-80 [39]. Homogeneity and conductivity of

the sample must be ensured to avoid false identifications and contamination. Limitations occur with some elements as nitrogen, oxygen, hydrogen, halogens, and noble gases are difficult to determine with OES [40]. Furthermore, the sample and chamber cleaning processes are easy as they can be done with a plastic brush and wire brush. Argon has an important role as it is an inert gas and displaces all the air and other particles in the chamber. It also allows the OES to detect light elements whose emitted wavelengths are below 200 nm [41]. Argon pressure is usually maintained in a range of 2000-3500 Pa depending on the device manufacturer and investigated samples [41].

3 Chemical analysis principles and classification

Chemical analysis can be divided into two main categories, qualitative and quantitative. Qualitative analysis provides information only on which elements are present as quantitative analysis provides also their amounts, which are typically presented in concentrations or mass fractions (wt%). In this study, all the results are presented in mass fractions. Quantitative analysis can be further performed with standards or use a standardless style as in this study. The standardless analysis is not comparable with standards-based analysis and it can lead to a wide range of systematic errors. Furthermore, this section covers the main indicators of the performance of the results: accuracy, precision, and different error types.

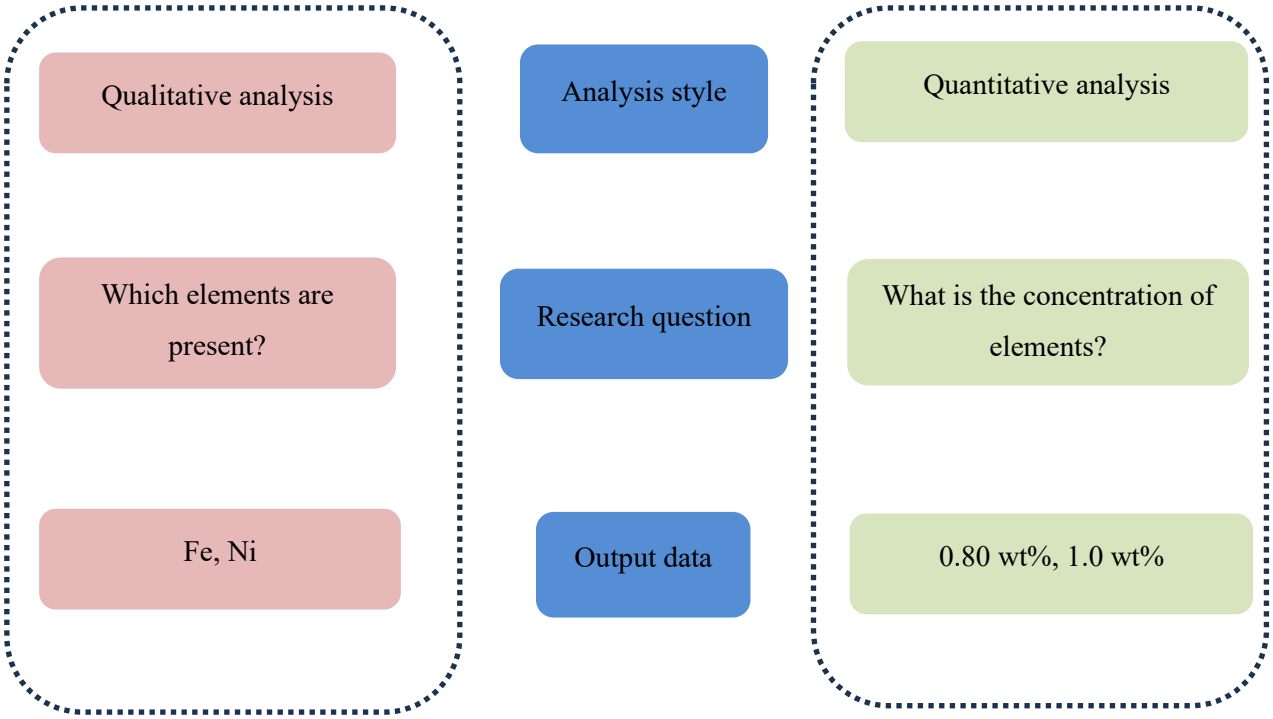

Figure 14. Illustration of the differences in qualitative and quantitative analysis.

3.1 Detection limits and light element detection

Limit of detection (LOD) refers to the lowest concentration of an element that can be detected from the sample and is not directly linked to the lightness of the element. Other terms and concepts that are commonly used to describe the lowest concentration of an analyte are limit of blank (LOB) and limit of quantification (LOQ) [42]. This thesis covers only LOD and LOQ as they are commonly used terms in elemental analysis. Terms can be varied depending on the analytical technique and can be calculated with the following formulas:

$$LOD = \frac{3.3\sigma}{S} \quad (3)$$

where σ is the standard deviation and S is the slope of the calibration curve. LOQ is calculated similarly but factor 3.3 in Formula 3 is replaced by factor 10. It refers to the lowest concentration of the analyte that can be consistently detected while meeting the predefined goals for bias and imprecision [42].

Light element identification is crucial for chemical analysis and materials science as it allows an in-depth understanding of material properties [43]. The key properties of various steel products are determined by the concentration and presence of the following trace elements: carbon, nitrogen, phosphorus, and sulphur [44]. These elements affect in mechanical and physical properties, for example ductility and stiffness, and only a small addition of carbon or nitrogen (around 1 wt%) is responsible of phase stability and microstructure of ferrous alloys. Light elements have energy levels that are low enough that they struggle to escape from the sample without being absorbed [45].

Especially the nitrogen detection has been complicated with the SEM-EDS technique as nitrogen (Z=7) belongs to the low Z elements (Z < 11) which are vulnerable to X-ray absorption phenomena [30]. Gazulla et al. studied two independent methods for analysis of nitrogen, which included SEM-EDS and elemental analysis by combustion and thermoconductivity detection [30]. Results were promising as SEM-EDS technique does not require decomposition of the sample which makes is suitable for materials that has a high decomposition temperature [30]. However, the LOD (0.5 wt%) and LOQ (1.5 wt%) values were significantly higher than the ones obtained by the elemental analysis [30].

3.2 Accuracy and precision

Major part of the elemental analysis is to understand the difference between precision and accuracy. Measurement accuracy is an important part of the analysis, and it refers to the results closeness to the true or reference value. To understand the inaccuracy behind the results, there are two parameters to determine: absolute error and relative error. Absolute error is related to the difference between true and measured value, and it can be calculated by subtracting the measured value from the true value. Relative error is closely related to absolute error, and it can be calculated as follows:

$$Relative\ error = \frac{|Measured\ value - True\ value|}{True\ value} * 100 \quad (4)$$

Precision relates to the repeatability of the measurement or certain method. The term is usually expressed with a coefficient of variation or relative standard deviation (RSD), which refers to the same parameter [46]. In this study, the precision of equipment is expressed with relative standard deviation, so it is crucial to understand the background of it. Two values are required to identify RSD: mean and standard deviation (SD) of the dataset. Mean is the arithmetic mean which is determined by calculating the sum of a set of numerical values and dividing it by the total number of values in the set. SD indicates the dispersion of the data in relation to the mean and it can be calculated as follows:

$$SD = \sqrt{\frac{\sum(x_i - \mu)^2}{N}} \quad (5)$$

where x_i is each individual data point, μ is the mean and N is the total number of data points [47]. RSD is calculated by dividing the SD by the mean and is usually multiplied by 100 as RSD is often expressed in percentages.

$$RSD = \left(\frac{SD}{\mu}\right) * 100 \quad (6)$$

where SD is the standard deviation and μ is the mean of the dataset. In conclusion, SD and RSD indicate the same thing in a different way, as SD is an absolute value, and RSD is a relative value. However, the method precision is often expressed with RSD. Figure 15 illustrates the previously mentioned difference between accuracy in more understandable and graphical way.

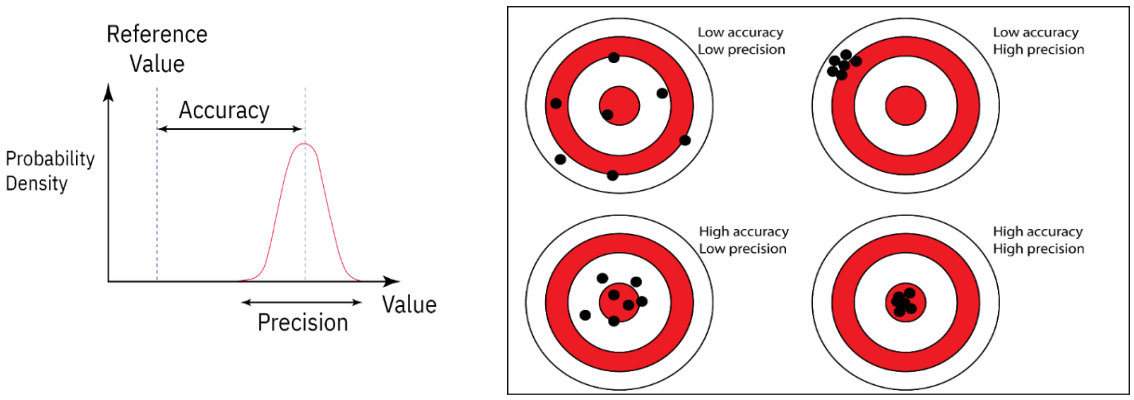

Figure 15. Graphical illustrations of the difference between accuracy and precision. Images reproduced from [48, 49].

3.3 Error types

Errors are an unavoidable part of measurements which can occur from many sources and in different forms in chemical analysis. The top three error sources in chemical analysis are sample preparation, human error, and equipment problems [50]. Sample preparation is also a human-based error so 2 out of 3 of the top three error categories are caused by human. Human errors can be further divided into random and systematic errors (Figure 16). A proper analysis of errors can increase the quality of the study and make the reader convinced about the reliability of the data. [44]

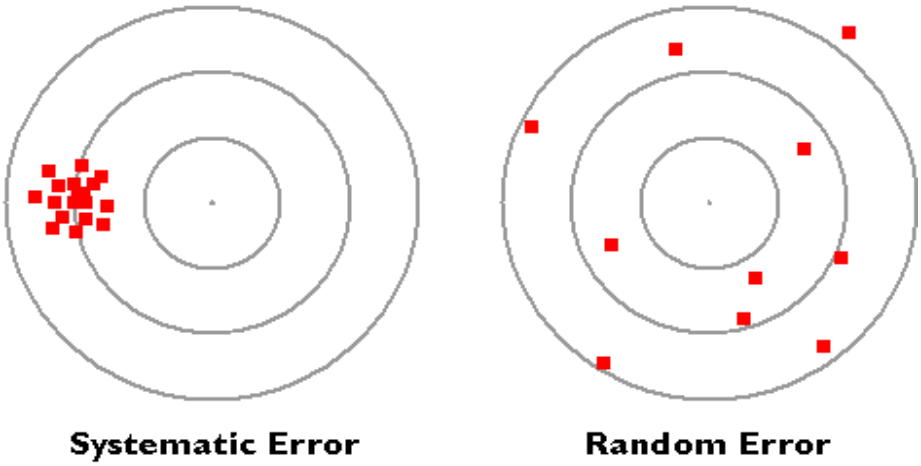

Figure 16. Comparison between random and systematic errors. Systematic errors result in clustered data points in the same spots which indicate that the error repeats in the same way. Random errors result in widely spread data points which indicate that the error causes may vary. Image reproduced from [52].

Random errors in chemical analysis are related to the precision of the method which results in high variance and widely spread data points [8]. The control of the random errors that are introduced by the sample preparation and analytical methods is important as it can improve the precision [8]. Systematic errors are related to the accuracy of the analytical results and they happen repeatedly in the same way resulting in low variance but high absolute error (Figure 16) [8].

A hypothesis is an important part of empirical research as well worked-up hypothesis is half the answer to the research question. Banerjee et al. studied the characteristics of a good hypothesis which should be simple, specific, and stated in advance [53]. Errors that are related to the hypothesis can be divided into type I error (false positive) and type II error (false negative) which both are types of inaccurate results [53]. False positives and false negatives can be avoided by using multiple methods, such as different analytical techniques.

The cause of error should always be identified even though errors can result randomly. Most of the errors are caused by the sample preparation process so it should be always carried out with a careful and specific protocol that is easy to follow. Contamination can be avoided with correct tools and manufacturer instructions should be followed to ensure the optimal use of equipment. Furthermore, when the research requires many samples with different materials rushing with the process should be avoided.

4 Purpose and objectives of the experimental part

The experimental part of this study aims to answer the open questions related to Wärtsilä Investigation Laboratory research equipment. The goal is to determine the optimal parameters and measuring conditions for each device. In addition, researching the best equipment for certain purposes of use. This is done through different surface qualities and materials.

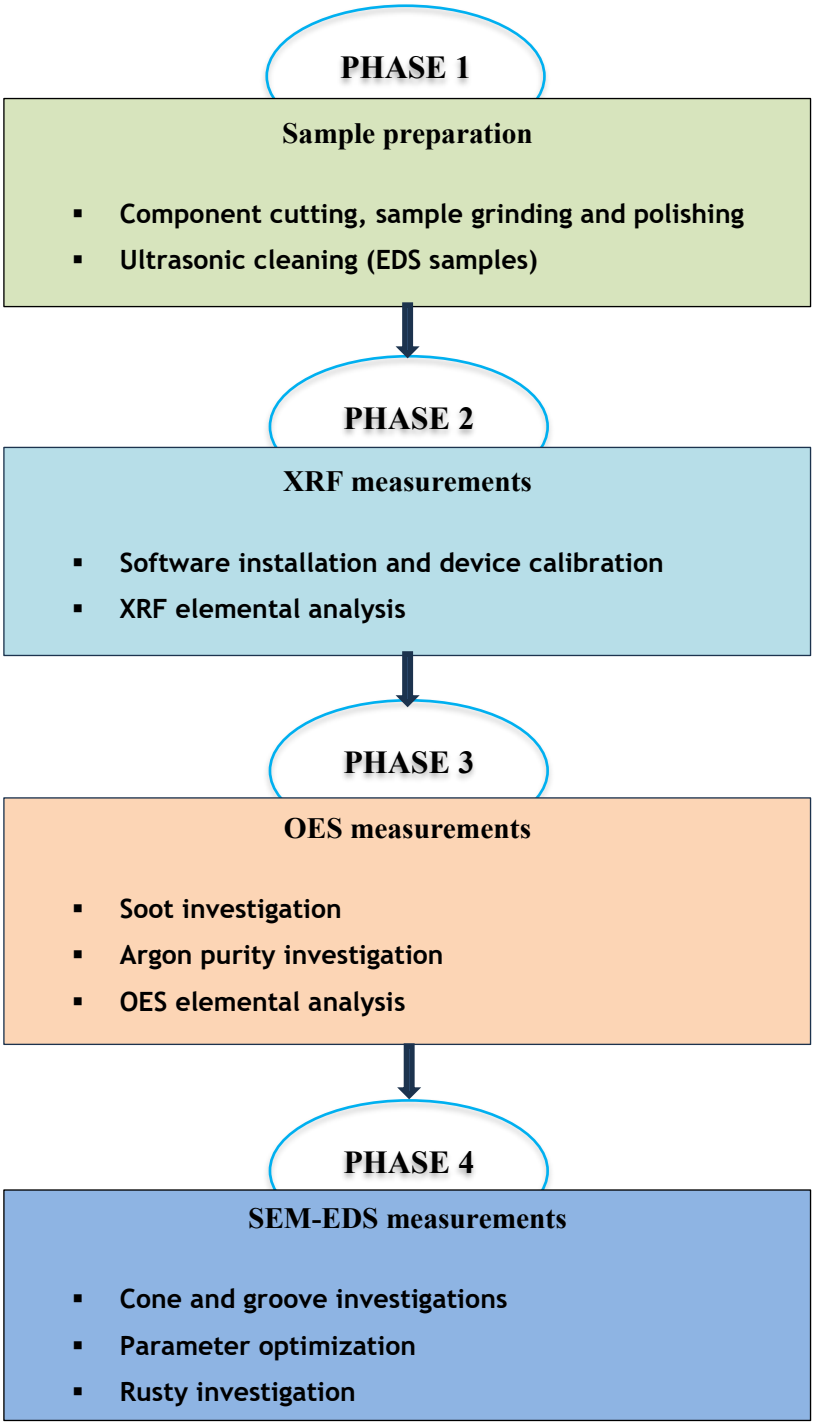

Figure 17. Separation of different phases in experimental part.

5 Experimental procedure

Table 1 presents every research and sample preparation device with images and application descriptions. This study included also other cutting machines and a mounting press but only the most essential devices for the work were chosen to be introduced in more detail.

Table 1. List of equipment used in this research. Pictures of sample preparation equipment are used with permission of Wärtsilä Turku Investigation Laboratory.

Equipment	Picture	Purpose of use
TESCAN VEGA3 with Thermo Scientific EDS-detector	 [54]	High-resolution imaging and elemental composition measurement
Olympus Innov-X Delta XRF analyzer	 [55]	Elemental composition measurements
Hitachi FOUNDRY-MASTER Smart	 [56]	Elemental composition measurements

Buehler Delta Automatic Abrasive Cutter		Component cutting
Struers Tegramin-30 grinding and polishing machine		Surface grinding to the desired surface quality
FinnSonic M3 ultrasonic cleaner		Washing SEM-EDS samples
Column drilling machine		Drilling the cones

5.1 Materials used

Materials to be used in this study were selected from common marine engine components and their intended chemical compositions are presented in Tables 2, 3, and 4. Values are taken from the Total Materia database. Three materials for comparison included copper, nickel, and iron alloys. Iron is not included in Table 4, but it is the main element of the alloy. The purpose of using different materials is to investigate the possible differences when detecting elements with various research devices.

Table 2. Chemical composition of CuAl10Fe5Ni5-C (copper alloy), data collected from Total Materia. [57]

Material		Al %	Bi %	Cr %	Cu %	Fe %	Mg %	Mn %	Ni %	Pb %	Si %	Sn %	Zn %
CuAl10Fe5Ni5-C	Max	10.5	0.01	0.05	83	5.5	0.05	3.0	6.0	0.03	0.10	0.10	0.5
	Min	8.5			76	4.0			4.0				

Table 3. Chemical composition of NiCr20TiAl (nickel alloy), data collected from Total Materia. [58]

Material		Al %	B %	C %	Co %	Cr %	Cu %	Fe %	Mn %	Ni %	P %	S %	Si %	Ti %
NiCr20TiAl	Max	1.80	0.008	0.10	1.00	21.0	0.20	1.5	1.00		0.020	0.015	1.00	2.70
	Min	1.00		0.04		18.0				65.0				1.80

Table 4. Chemical composition of 34CrNiMo6 (iron alloy), data collected from Total Materia. [59]

Material		C %	Si %	Mn %	P %	S %	Cr %	Ni %	Mo %
34CrNiMo6	Max	0.38	0.40	0.80	0.025	0.035	1.70	1.70	0.30
	Min	0.30	0.10	0.50	0.000	0.000	1.30	1.30	0.15

5.2 Sample preparation

It is crucial to understand the important role of sample preparation in chemical analysis. Even minor impurities, such as fingerprints can have a major impact on measurement results. At low concentrations, these impurities can lead to significant errors. The sample preparation followed the standard procedure for failure analysis cases at Wärtsilä and is described in more detail for each sample. Table 5 provides an overview of every sample investigated in this study, and the

number of measurements for each device. Naming is in alphabetical order as K refers to copper, N for nickel, and R for iron, and the same trend continues throughout the thesis. Samples were photographed with a system camera, including shooting lights to obtain high-quality images.

Table 5. Explanation of the naming principle for each sample including images and number of measurements.

Description	Reference sample	Sample with cone and groove	Fracture surface sample	80 polished sample
Sample ID	K1	K2	K3	K4
Image	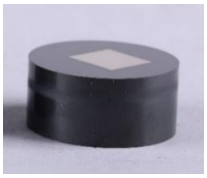	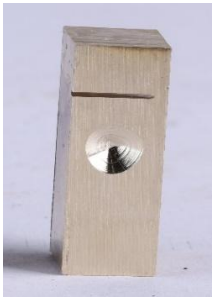	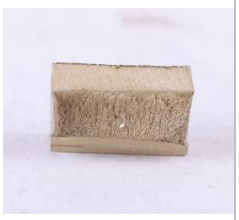	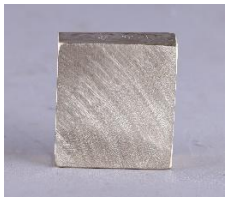
Device	EDS, XRF	EDS	EDS	EDS / XRF
Quantity	3 (EDS) 10 (XRF)	25	3	3 (EDS) 10 (XRF)
Sample ID	N1	N2	N3	N4
Image	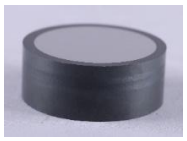	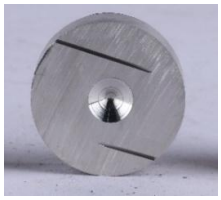	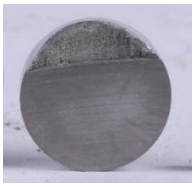	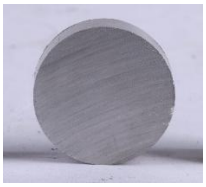
Device	EDS / XRF	EDS	EDS	EDS / OES / XRF
Quantity	3 (EDS) 10 (XRF)	25	3	3 (EDS) 30 (OES) 10 (XRF)
Sample ID	R1	R2	R3	R4
Image	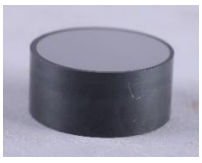	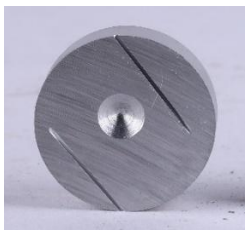	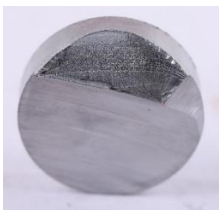	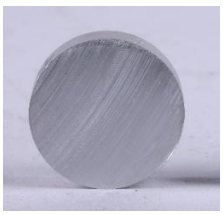
Device	EDS / XRF	EDS	EDS	EDS / OES / EDS
Quantity	3 (EDS) 10 (XRF)	25	3	3 (EDS) 30 (OES) 10 (XRF)

Component cutting was done with an automatic abrasive cutter. Sample names ending with number 1, 2, and 4 were cut to a thickness of 10 mm. To simulate a real fracture surface, the remaining part of each component was cut almost all the way through, then clamped in a vice and fractured using a sledgehammer to produce an authentic fracture surface. Subsequently, these samples were also cut to a thickness of 10 mm. Each device in the study has specific requirements for optimum surface quality and sample size, and the aim was to investigate the effect of different surface qualities. The following sections detail the preparation method for each of the four samples.

The sample buttons K1, N1, and R1 were prepared using a hot mounting press, where the sample was embedded in Polyfast-mass which is commonly used for SEM examination. The sample to be mounted was placed in the press, after which Polyfast was dispensed on top of it. After that, the sample was sealed inside the press and the correct temperature and compression force were ensured. The duration of the program was 9 minutes, with a temperature of 180 °C and 30 kN pressing force. Mounting was followed by a 6-minute cooling program. The surface was prepared with a polishing machine with Struers MD-Dac 3 µm polishing disc.

There was also interest in investigating samples with cones and grooves (K2, N2, and R2). Cones were made with a column drilling machine with a 10 mm twist drill. The grooves were made accordingly with a precision cutter and 0.8 mm thick cut-off wheel. These samples were only for the SEM-EDS investigations since the XRF measurement area is too large for samples of this size and OES is not suitable for samples of this shape.

OES requires relatively rough surface quality and for this reason, the samples K4, N4, and R4 were ground with Struers Piano MD 80 grinding plate. The grit size was 80 and the grain size was 200 µm. After this, the samples were washed with alcohol and dried with a hot air blower. The direction of grinding grooves had to be equal as intersecting grooves would possibly affect negatively on the results.

5.3 Internal accuracy measurements

XRF results were obtained for every material but only samples with sequence numbers 1 and 4. The amount was 10 measurements per sample. The surface needs to be flat and larger than the XRF measurement area (4 cm x 4 cm) so the fracture surfaces, holes, and grooves could not be measured. Exception to this was sample K1, which was measured despite being smaller than the convenient sample size. Prior to the measurements, each sample was ground (following the

guidelines in chapter 5.2), washed in alcohol, and dried. The study focused on the same area of the sample, as the purpose was to obtain measurement accuracy and precision. To ensure consistency, XRF was attached to a stand on the table, with the measurement window facing upward (Figure 18). After that, the sample was placed on top of the measurement window and the lid of the box was closed so that the X-ray radiation emitted by the device could not escape. XRF was always calibrated with the devices own standard sample before starting the measurement series. The measurements were controlled with Delta Advanced PC software. It belongs to the same product family as the Innov X Delta XRF analyzer. Figure 18 illustrates the measurement arrangements for this phase.

Figure 18. Measurement arrangements for XRF in desktop-mode. The ‘analyzer is attached to the table stand and measurement window is pointing upwards inside the box.

In this study the used spark OES was Hitachi Foundry Master Smart. Measurements started by fine-tuning the device settings and operation. Before starting the measurements, an optic flush had to be performed, which takes 30 minutes. It is the device's own cleaning system that fills the system with Argon, and it should always be used when the OES has been out of use for a few days. In this study, the optic flush was always done if the measurements were on separate days. There is also another similar function which is called Argon flush. It is included in the sparking program, but it can also be operated by the user. It works similarly with optic flush, but the Argon flow rate is higher, and it is recommended to use for a few minutes before measurements. When using these functions Argon flows inside the system and all the possible particles, impurities and off-gases are removed to a washing bottle (filled with tap water) which is connected to the system with a flexible hose (Figure 19).

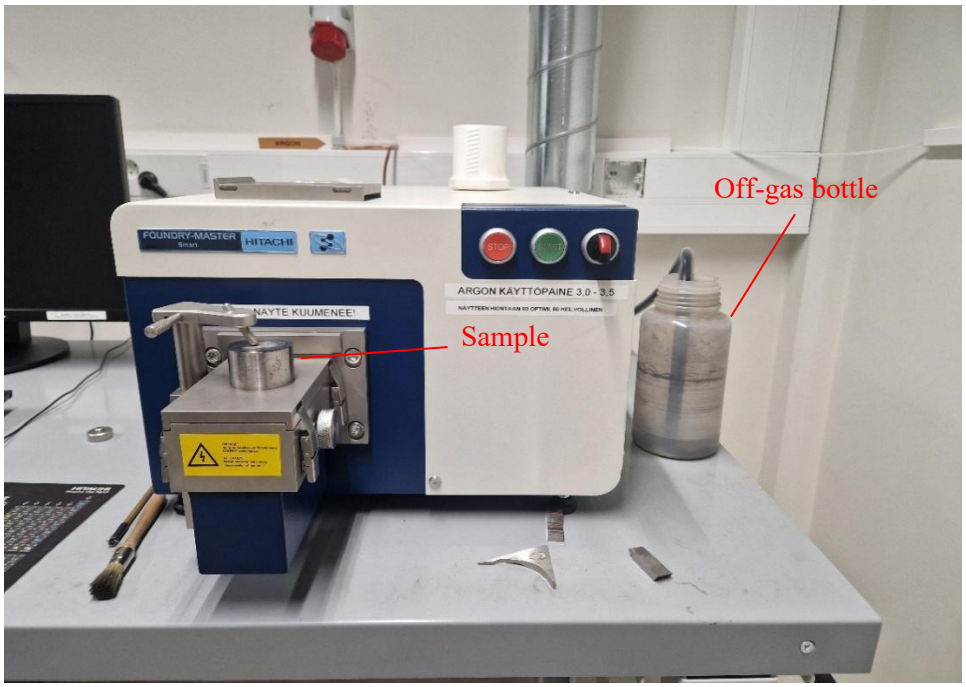

Figure 19. Measurement arrangements for OES including sample and off-gas washing bottle on the right side. The sample was placed on a spark stand and the process was operated with a computer.

The first investigation was related to the effect of soot in the chamber, especially to the measured carbon concentration. Previous studies in this laboratory have shown that the amount of carbon is too high in the first measurements when using the laboratory's control test sample. After this, the amount of carbon is slowly decreasing to the determined standard level. This phenomenon was studied by making two different series of measurements with a test sample. Surface grinding was done according to chapter 5.2, and then samples were washed in alcohol and dried carefully. Before sparking the sample, the chamber and spark electrode were cleaned with a coarse mop and wire brush. After that, the sample was placed on the spark stand, as shown in Figure 19. The device was controlled using Hitachi SparcFire software.

The first series of soot investigation consisted of a total of 21 (7+7+7) measurements and after every seven measurements the chamber and spark electrode were cleaned. The second series contained 21 measurements in a sequence without cleaning. Both series were done without an additional Argon flush function. Additional research was done to investigate the effect of longer use of the Argon flush function on the amount of measured carbon. The hypothesis behind this is that it should completely purify the system and decrease carbon fluctuation. This section consisted of 30 measurements (10 + 10 +10), in which an additional 5 min Argon flush was performed on the device before each series. In the second phase, air was allowed to flow deliberately into the chamber for five minutes, after which measurements were taken immediately.

Table 6. Explanation of different measurement series with OES.

Type of measurement	Sample	Number of measurements
Soot investigation	Test sample	21 (7+7+7)
Soot investigation	Test sample	21 (in a row)
5 min Argon flush	Test sample	30 (10+10+10)
Chamber open for 5 minutes	Test sample	30 (10+10+10)
Elemental analysis	N4	30 (10+10+10)
Elemental analysis	R4	30 (10+10+10)

The comparative research between different materials was done on nickel and iron alloys with 30 measurements per sample. This stage was performed in sets of 10, followed by equipment cleaning and sample grinding. For the nickel-based material, a specific spark electrode and cleaning brush were utilized to prevent contamination. Argon pressure was maintained around 3000 Pa during every measurement. To prevent air from entering the chamber, the sample was rotated without lifting it, to obtain a slightly different spot to study. There was no program for copper-based material so copper-alloy samples were not measured with OES.

EDS measurements were made for all materials, and the used parameters were same as in typical failure investigation case in Wärtsilä Turku Investigation Laboratory. Accelerating voltage was 20 kV, working distance was 15 mm and beam intensity was 12. EDS parameters were the following: live time limit of 30 seconds, dead time of 2 %, and rectangle-shaped investigation area. Optimization for these parameters was done in separate measurements which is presented further in this thesis.

The procedure for sample preparation was to polish samples always before starting the measurement. SEM has different requirements than XRF and OES as the samples had to be cleaned with alcohol in ultrasonic cleaner after polishing. The drying process was done with a hot air blower. A dry sample is crucial as the SEM operates in a high vacuum, which can cause evaporation if the sample is wet. All EDS samples were washed and dried similarly.

The grooves were marked to indicate measurement depth of 1 mm to ensure consistency. Markings were engraved with a Dremel. Figure 20 shows the measurement areas and the position of the EDS detector with the groove. Measurements were taken from 8 directions by rotating the sample clockwise. The samples with cones were studied as shown in Figure 21 and

a total of 9 measurements were performed from each sample (K2, N2, R2). Detector position is marked to both groove and cone measurement arrangements illustrations (Figure 20 and 21).

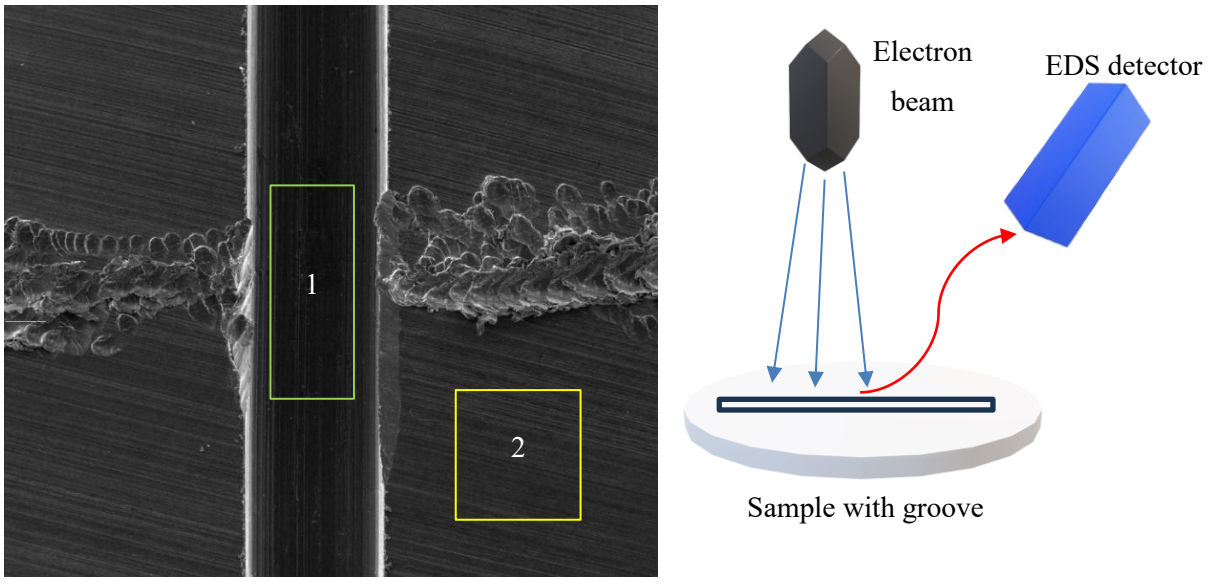

Figure 20. SEM image of measurement spots for samples K2, N2, and R2 (left side). On the right side is an illustration of the position of the EDS detector relative to the groove.

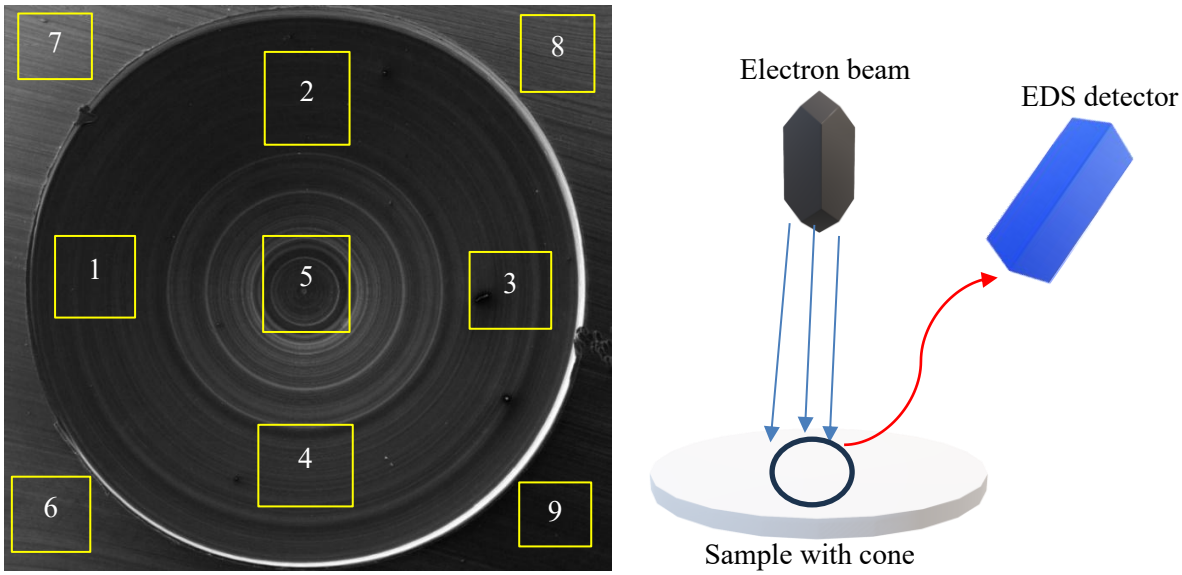

Figure 21. SEM image of measurement spots for the cone in sample N2 (left side). On the right side is an illustration of the detector alignment when analyzing the cone.

Another important research problem was the optimal parameters, especially for SEM-EDS. The studied parameters were dead time, absorption current, and beam intensity which controlled with SEM. Accelerating voltage was 20 kV, working distance 19 mm, and the live time limit increased to 50 seconds. The measurement area was switched from rectangle to point. Parameter adjusting was done with three different samples (K1, N1, and R1) to investigate the possible differences in mass-percentages, integral counts, and RSD values. The number of

measurements was 6 for every sample and the points were randomly selected. Furthermore, to find the most accurate and precise setup, another study with only one measurement spot was needed. In this phase, EDS analysis was performed 6 times but exactly from the same spot of the sample. This should eliminate the fluctuations and result in lower RSD values.

Table 7. Different parameters for investigation of the optimal setup for elemental analysis with SEM-EDS. Working distance (19 mm) and accelerating voltage (20 kV) were held constant.

Absorption current (nA)	Beam intensity	Dead time (%)
0.56	14	6
1.0	15	10
1.6	16	16
2.1	17	20

The impact of rust in EDS measurements was investigated by intentionally rusting two fracture surface samples consisting of iron alloy. The purpose was to achieve deep corrosion which is not completely flushed away in ultrasonic cleaning. Both samples were placed in separate receptacles for two weeks in the presence of water (Figure 22). After one day, half a tablespoon of salt was added to sample A (Figure 22) to accelerate the rusting process. Receptacles were sealed with packing tape. Measurements were performed with 20 kV accelerating voltage, beam intensity of 15, working distance of 19 mm, absorption current of 1.5 nA, and dead time around 10 %.

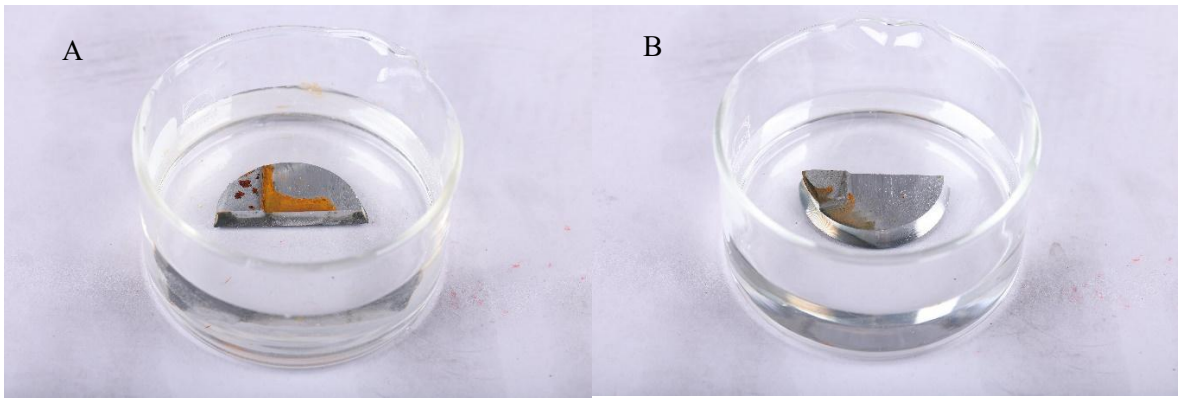

Figure 22. Samples A and B before sealing.

5.4 Theory studies for the experimental part

The experimental part contained a few theory studies and investigations, on the initiative of Wärtsilä, to obtain more experience-based information related to use and operation of analytical techniques. For detailed theory studies were selected the following research questions:

- How harmful is wet/oily sample to SEM?
- How to reduce image distortions generated by electromagnetic interference (EMI) in SEM?

These questions were opened by studying relevant literature and searching for articles related to the topics.

6 Results and discussions

In this section, the accuracy and precision results for XRF and OES are presented and analyzed. EDS results are presented in a separate section after the internal accuracy part as the focus was on the surface qualities and optimal parameters. Precision is expressed as relative standard deviation, which is calculated according to Formula 6 (page 26). In addition, mean and standard deviation (SD) for the results are calculated to support precision calculations. Accuracy is presented in terms of match-%, which tells the percentage of detected elements whose amount is in the standard range. At the end of this section, there is a comparative review and an analysis of the most suitable device for certain purposes of use.

6.1 Internal accuracy analysis and results

The analysis consists only of the detected elements and for clarity, only these standard values are presented in Tables 8, 9, and 10. Every analysis technique detected elements that are not included in the standard, so these were intentionally left outside the analysis. In addition, Fe wt% is not included in the results for R1 and R4 samples as it is the main element of the alloy and has no value in the standard.

6.1.1 XRF results and analysis

In the copper-based samples K1 (Table 8) and K4 (Table 8), most of the reference elements were not detected, resulting in only 50 % detection rate. This results from low concentrations of elements that XRF cannot reliably detect. The RSD values remained relatively low (< 5 %) and only the amount of silicon varied a lot, which resulted in high RSD values (Table 8).

Table 8. XRF wt% and precision results for K1 and K4 samples. Wt% are averages calculated from 10 sets of measurements.

Elements	Standard values (wt%)	K1 (wt%)	RSD (%)	K4 (wt%)	RSD (%)
Al	8.5–10.5	8.71	1.56	9.17	2.83
Cu	76.0–83.0	82.03	0.17	81.49	0.32
Fe	4.0–5.5	3.75	0.72	3.75	1.05
Mn	≤ 3.0	0.28	4.91	0.27	4.83
Ni	4.0–6.0	5.11	0.97	5.13	1.50
Si	≤ 0.1	0.11	15.2	0.14	12.5

In the N1 sample, the XRF detected Mn only one out of ten times, which falsified the results, as the mean value is calculated from one test result. This was the reason to leave it completely out of the result analysis. This increases the measurement uncertainty, as in the N4 sample XRF detected Mn within reference values in every measurement. The deviation of aluminium is higher than in the copper alloy samples.

Table 9. XRF wt% and precision results for N1 and N4 samples. Wt% are calculated averages from 10 sets of measurements.

Elements	Standard (wt%)	N1 (wt%)	RSD (%)	N4 (wt%)	RSD (%)
Al	1.0–1.80	1.54	7.38	1.64	12.03
Cr	18.0–21.0	18.76	0.67	18.84	0.80
Fe	≤ 1.5	0.67	2.35	0.67	6.54
Mn	≤ 1.0	*		0.18	3.25
Ni	≥ 65.0	76.89	0.72	77.01	0.95
Si	≤ 1.0	0.14	16.08	0.17	7.56
Ti	1.8–2.7	2.03	5.42	2.02	2.62

*Mn was left out of N1 results since it was detected only once.

Iron alloy samples R1 and R4 gave precise results except for phosphorus (P) and copper (Cu) which deviated a lot resulting in RSD values of 15.7 and 23.7. Copper was detected only 2 times out of 10 measurements. High RSD values are again due to elements with low concentration (minor and trace elements). Overall performance was good as almost every other RSD value remained under 6.

Table 10. XRF wt% and precision results for R1 and R4 samples. Wt% are calculated averages from 10 sets of measurements.

Elements	Standard (wt%)	R1 (wt%)	RSD (%)	R4 (wt%)	RSD (%)
Cr	1.30–1.70	1.48	3.31	1.46	2.16
Mn	0.50–0.80	0.62	4.55	0.63	4.71
Mo	0.15–0.30	0.16	2.83	0.16	2.98
Ni	1.30–1.70	1.26	4.42	1.27	2.80
P	≤ 0.025	0.03	23.7	0.03	11.09
Si	≤ 0.40	0.41	4.88	0.44	6.13

Based on the results in Tables 8, 9, and 10, it can be concluded that the surface quality had no significant effect on the measurement results. There was a little deviation between MD-Dac 3 µm (K1, N1, R1) and MD-Piano 80 (K4, N4, R4) samples, but no clear consistency was found.

It was noted that higher concentrations generally resulted in more precise and accurate results for each material. However, this trend does not happen systematically, as lower RSD values were sometimes observed despite lower element concentrations. Furthermore in the ideal situation, also the intensity of an analytical line would be directly proportional to the concentration of the element in the sample [8].

6.1.2 OES results and analysis

OES detected elements that were not in the material standards, but the concentrations were relatively low. The main purpose was to focus on the elements present in the standard, so these additional findings were left without attention. Measurements with N4 and R4 samples indicated similar elevated levels in the carbon concentration, which decreased when more burns were performed. To compensate this the results shown in Tables 11 and 12 have been taken from the last 5 measurements of each series. At this point, the fluctuation of carbon has been smoothed out. In these tables the focus is on RSD values and the lower the better. Overall RSD values are low, and high values occur only with elements with low concentrations (≤ 0,008 wt%). This supports the assumptions of OES as the most accurate device in this laboratory.

Table 11. OES wt% and precision results for sample N4. This investigation consisted of three series with 30 measurements (10+10+10). The wt% for the results table are calculated from the averages of the last 5 measurements of each series to eliminate the effects of carbon fluctuation.

Elements	Standard (wt%)	N4 (wt%)	RSD (%)	N4 (wt%)	RSD (%)	N4 (wt%)	RSD (%)
Al	1.0–1.8	1.36	0.52	1.36	0.40	1.38	0.32
B	≤ 0.008	0.0063	17.9	0.0056	2.73	0.0055	3.48
C	0.04–0.10	0.058	3.04	0.056	0.67	0.053	2.18
Cr	18.0–21.0	17.7	0	17.5	0.31	17.1	0.87
Cu	≤ 0.20	0.003	2.91	0.003	3.23	0.0029	10.2
Fe	≤ 1.5	1.12	0.49	1.12	0	1.13	0.001
Mn	≤ 1.0	0.07	0.91	0.068	0.86	0.066	4.5
Ni	≥ 65.0	77.2	0.07	77.4	0.06	77.9	0.19
Si	≤ 1.0	0.04	1.70	0.04	2.69	0.04	4.03
Ti	1.8–2.7	2.24	0.91	2.21	0.81	2.16	1.31

Table 12. OES wt% and precision results for sample R4. This investigation consisted of three series with 30 measurements (10+10+10). The wt% for the results table are calculated from the averages of the last 5 measurements of each series to eliminate the effects of carbon fluctuation.

Elements	Standard (wt%)	R4 (wt%)	RSD (%)	R4 (wt%)	RSD (%)	R4 (wt%)	RSD (%)
C	0.30–0.38	0.349	1.70	0.34	1.07	0.339	1.08
Cr	1.30–1.70	1.48	1.07	1.45	0.69	1.43	0.31
Mn	0.50–0.80	0.58	0.85	0.58	0.56	0.57	0.26
Mo	0.15–0.30	0.17	1.80	0.17	0.88	0.17	0.32
Ni	1.30–1.70	1.27	0.43	1.28	0.43	1.29	0.43
P	≤ 0.025	0.0076	14.9	0.0096	13.9	0.0101	7.47
S	≤ 0.035	0.0058	11.4	0.0052	7.94	0.0053	6.70
Si	≤ 0.40	0.32	1.94	0.32	0.80	0.32	0.49

This study did not include calibration as the standard samples were not available, so the calibration curves cannot be presented here. Therefore, these results are not fully comparable with other studies where the calibration has been performed. The lack of calibration leads to slightly less accurate results and the standardless analysis style makes it more complicated to compare with other studies. However, the obtained results align with the study of Zhang et al. and the data gives an understanding of the current state of analytical performance of OES in the Wärtsilä Turku Investigation Laboratory [39]. The comparison of the results from Zhang et al. and this study are shown in Table 13 [39].

Table 13. Comparison of the precisions between two different spark OES and LIBS from separate studies [39]. Materials and concentrations are different, but the elements are the same. Values for Lab Spark 750 and LIBS-OPA 100 are from [39].

Elements	Sample R4 (wt%)	RSD (%)	Lab Spark 750 (wt%)	RSD (%)	LIBS-OPA 100 (wt%)	RSD (%)
C	0.339	1.08	0.427	0.81	0.410	2.37
Si	0.32	0.49	1.13	0.93	1.12	2.18
Mn	0.57	0.26	0.800	0.74	0.802	2.23
P	0.0101	7.47	0.021	3.1	0.017	5.12
S	0.0053	6.70	0.020	5.2	0.024	9.34
Cr	1.43	0.31	1.07	1.05	1.08	2.13
Ni	1.29	0.43	0.414	0.63	0.421	1.92

The biggest variation in relative deviations is noticed with elements P and S. On the other hand, the concentrations are around 30 % smaller in this study. Other values are more similar and for

Si, Cr, Ni, and Mn the RSD values are lower than in the study of Zhang et al. [39]. However, the comparison of results is only indicative as the measurement parameters and devices are different, surfaces are polished differently, and the other study is performed with calibration.

The carbon fluctuation phenomenon has been problematic in previous investigations in Wärtsilä Turku Investigation Laboratory. The same phenomenon occurred in this study as the carbon concentration varied aggressively in each measurement series. There was a significant drop in carbon percentage between the first and the last measurement of each series with a decrease up to 13 %. Carbon level increased again after cleaning the equipment and this trend continued unchangeable in the third phase. (Figure 23)

Correspondingly, in the test where the electrode was not cleaned after every seven measurements (yellow line in Figure 23), the carbon level remained significantly more constant. Furthermore, the RSD value decreased by 59 % compared to the first measurement and the carbon level remained within the reference limit values throughout the measurement. Soot accumulates on the electrode during the measurement, because it burns the surface of the sample. In theory, this should increase the carbon level, as the soot mostly contains carbon. The soot investigation did not follow this line, so further studies were required to understand the root cause of the change in the amount of carbon.

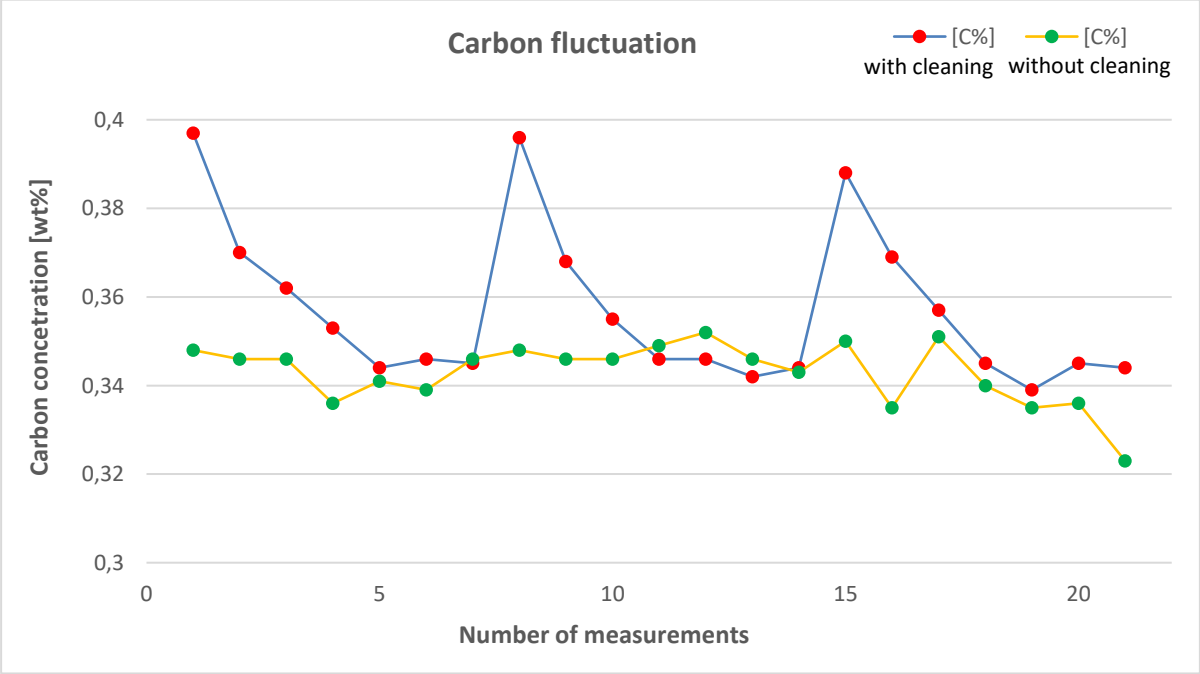

Figure 23. Carbon fluctuation during two different measurement series for the OES test sample. The blue line with red dots shows the results when the chamber was cleaned after 7 measurements and the yellow line with green dots indicates the results without cleaning. Both series consisted of a total of 21 measurements. Standard wt% value range is 0.30-0.38.

After mixed results from the soot test, it was necessary to look more broadly at the factors affecting the change in the amount of carbon. The effect of additional 5 minutes use of Argon flush compared to 5-minute intentional air flow to chamber was investigated and it was noticed that if there is air left in the chamber, the starting level of carbon is higher and decreases as more measurements are performed (Figure 24). This decrease is due to increased Argon that is pumped in the chamber in which case it displaces any air that may remain there. In addition, the amount of carbon remains more constant throughout the measurement series. This is supported by the Hitachi OES manual as it states that if the Argon quality is 99,996 % or less, the analysis is remarkably inaccurate.

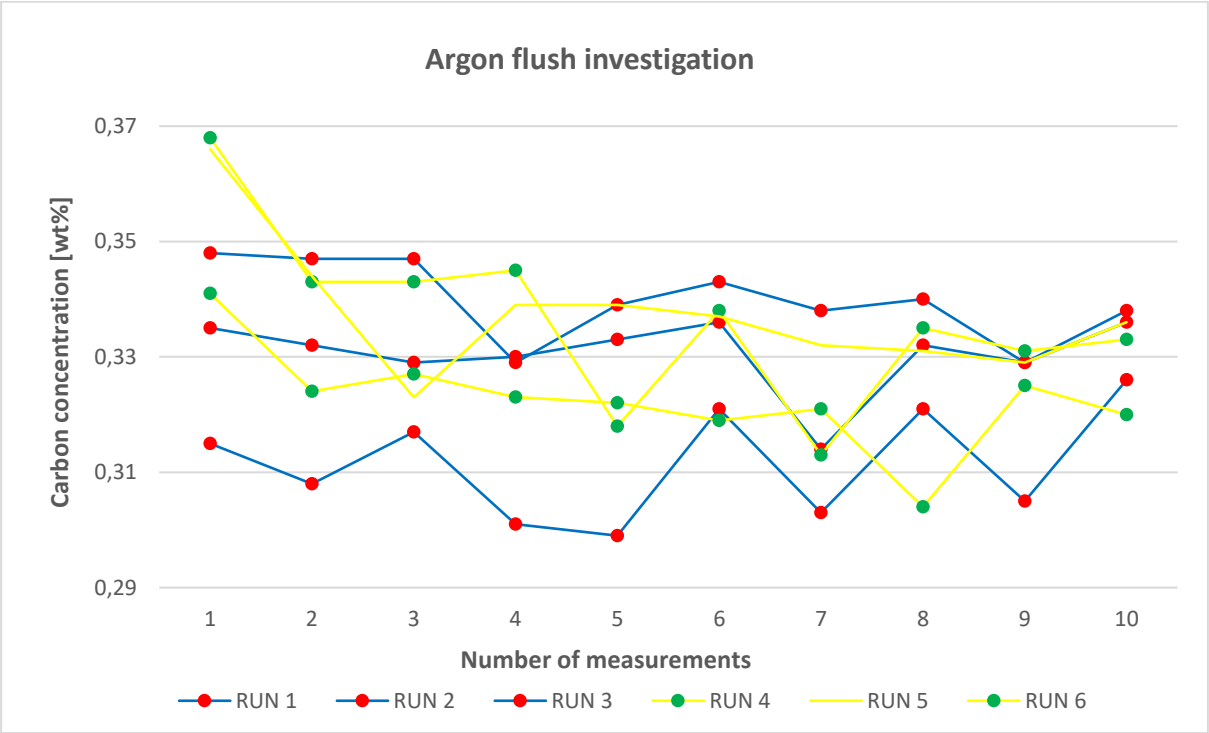

Figure 24. Illustrative graph of the carbon concentration propagation with 5 min Argon flush function compared to situation where the chamber was open for 5 minutes before measurements. Red lines with black dots (RUN1-RUN3) indicate the measurements with 5 min Argon flush and blue lines with pink dots (RUN4-RUN6) indicate the measurements with chamber open for 5 minutes before starting. Standard wt% value range is 0.30-0.38.

These results refute previous theories that increased soot was the reason why the carbon content decreased as the measurement progressed. Although this study examined the effect of Argon concentration only on the amount of carbon, it was found to have no significant effect on the concentrations of other elements. The same trend with carbon was observed also in measurements with the N4 sample. To achieve accurate results constantly further development ideas are discussed in chapter 6.4.

6.2 SEM-EDS parameter optimization and surface quality results

One drawback occurred in iron-alloy samples (R1, R2, R3, R4) as the EDS spectral resolution was not high enough to separate overlapping Mo L_α and S K_α peaks, which have emission energies close to each other (2.29 and 2.31 keV). Typical resolution for EDS is from 50 eV up to 150 eV depending on the spectrometer [33]. Better resolution appears in narrower peaks because the peaks can get closer to each other without overlapping. Figure 25 illustrates this phenomenon in the R4 sample, where Mo L_α and S K_α peaks cannot be separated. In elemental analysis this results in false identifications as most of the time, the S wt% turns 0 when manually selecting Mo and S active for EDS detection. This drawback could be handled with a WDS detector that has a better spectral resolution (2-50 eV) and it can resolve relative changes in energy in the range 0.01-0.1 which would be enough to solve mentioned Mo and S peaks (2.31 – 2.29 = 0.02 keV) [9], [34].

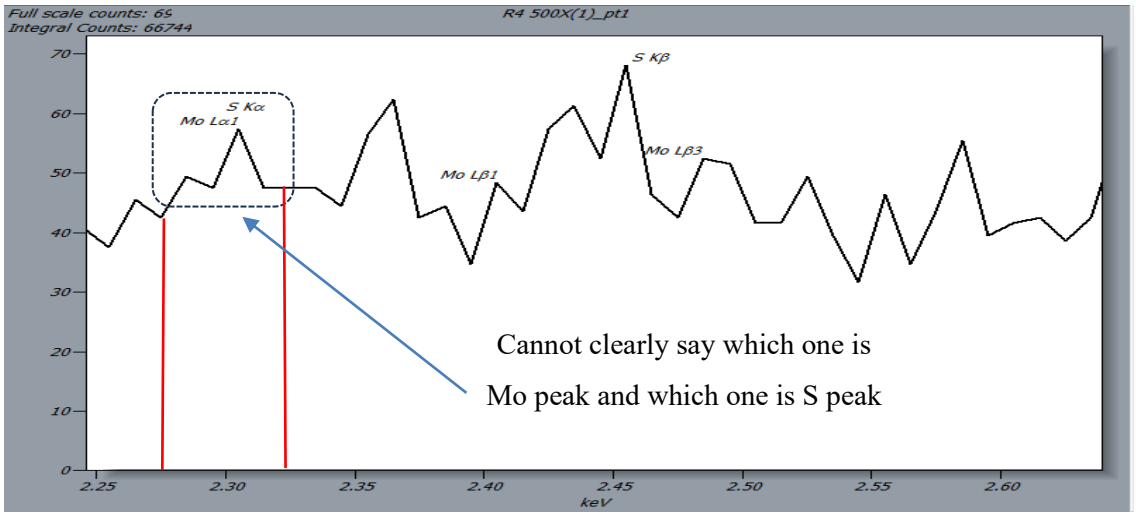

Figure 25. Overlapping Mo L_α and S K_α peaks in the area that is delimited with red lines (R4 sample). Peaks cannot be clearly separated from each other because the resolution of EDS detector is not low enough to resolve energy peaks that are this close (2.29 keV and 2.31 keV).

Adjusting SEM absorption current through different beam intensity values significantly impacts the results as the number of integral counts increased more than 10 times higher than previous parameter settings (Figure 26). This had also an impact on dead time which was from 6 % up to 20 % in this measurement. Before parameter adjusting the dead time was 1 % which resulted in low integral counts. It was noticed that the number of automatically identified elements by EDS increased and was constantly 7/9 for sample R1. In addition, the RSD values decreased. The most precise results were obtained when using the same measurement location and making multiple measurements to avoid random errors. The live time limit increase from 50 to 60 seconds did not make the results more precise.

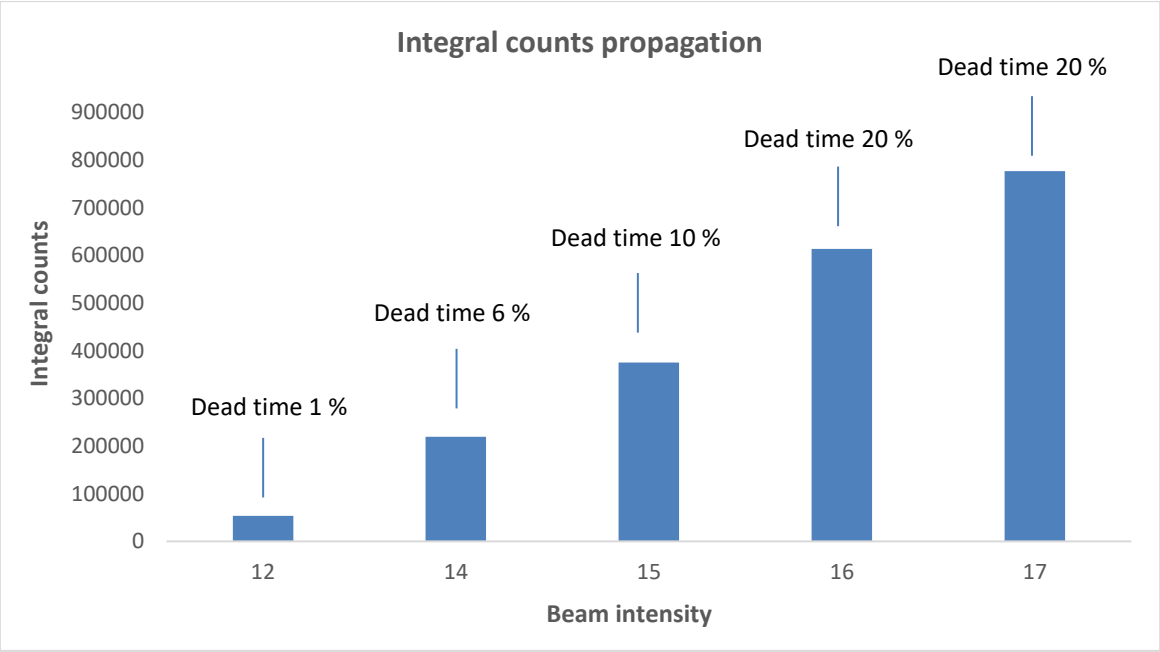

Figure 26. Integral counts comparison between different beam intensities. Dead time is also depending on the beam intensity, and it is shown above the data peaks.

Cone measurements indicated that the measurement spot has a major impact on the results. This is probably due to the low take-off angle which may interfere with the collection of X-ray photons emitted from the valley area for rough surfaces (Figure 27) [9]. Therefore, the emitted X-rays are blocked before they can be measured and detected with EDS. Figure 28 shows the integral counts distribution, where the counts remain continuously low at spots 4, 7, and 8. The number of integral counts remained low also in spots 7 and 8, which is surprising as those are on even surface and outside the cone. The reason for this is unknown as other spots outside the cone resulted in high integral counts. Hence it can be stated that if the sample contains a cone, the most reliable results are obtained from the bottom.

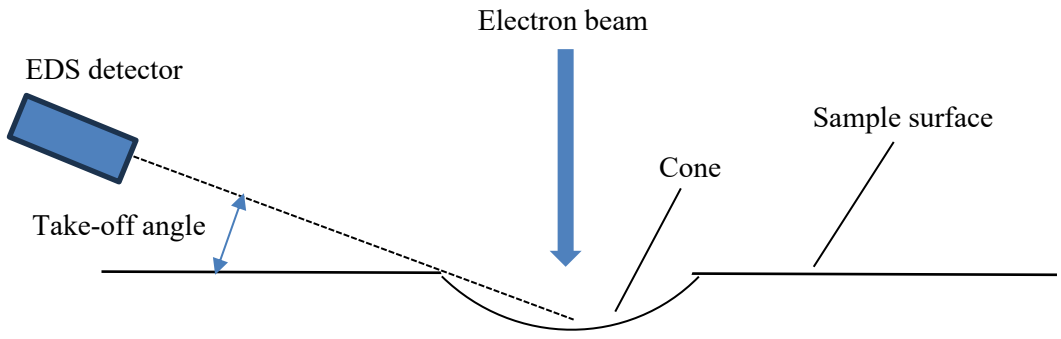

Figure 27. Illustration of the low take-off angle effects on measurements with cone. If take-off angle is too low the emitted X-rays from the bottom of the cone cannot be detected.

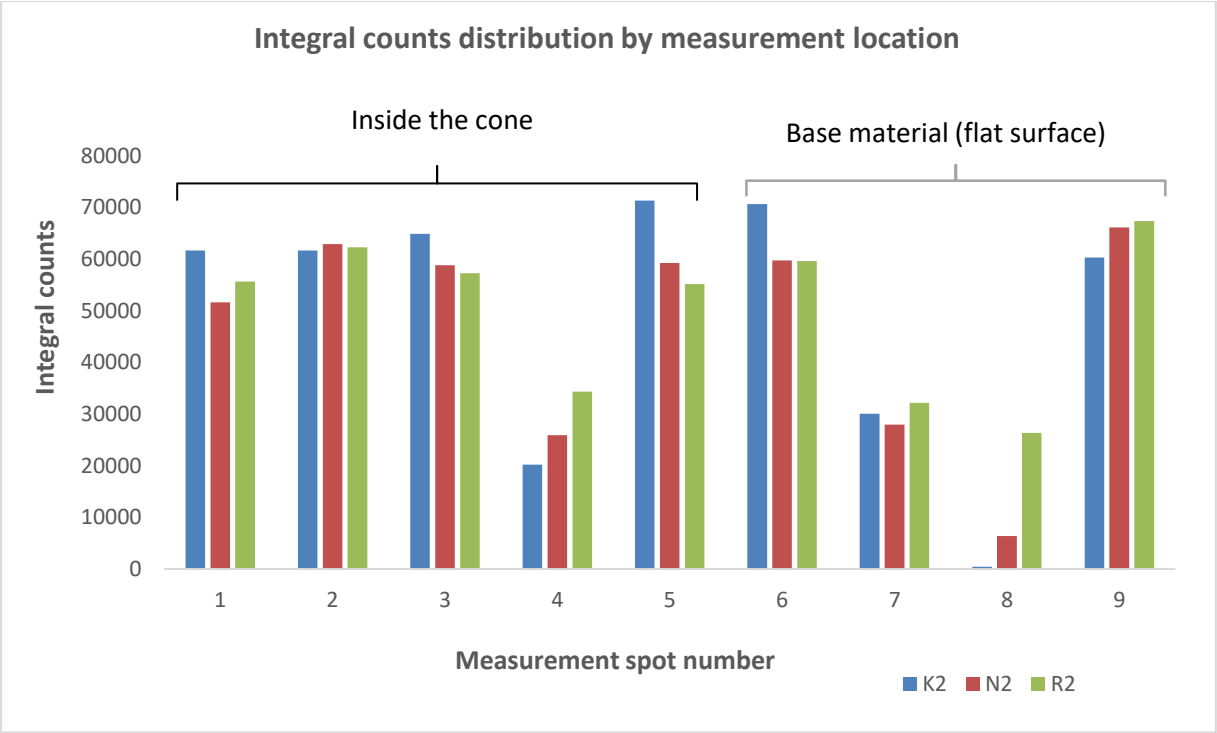

Figure 28. Integral counts in different spots in cone samples (K2, N2, and R2). Measurement spot has a significant impact on the number of integral counts inside the cone which can be seen in spot 4. Spots 7 and 8 are also resulting in low integral counts which is surprising since they are measured outside the cone.

Groove measurement indicated that it is essential to investigate the groove from the correct direction relative to the detector. There was a significant difference in intensity depending on the alignment of the groove. When the groove is horizontal, the intensity remains constant under 5000 counts (Figure 29). Furthermore, the integral counts in spots 7 and 8 are also low, even though those are on the flat surface of the sample. However, when the groove is vertically aligned, the intensity increases significantly, reaching up to 60,000 counts. A small number of integral counts results in poor quality and resolution of elemental analysis. Only major elements (copper, iron, and nickel) are detected as most of the emitted X-rays are blocked by the sample. These results indicate that the groove's correct alignment is essential for obtaining enough integral counts for elemental analysis. The samples with fracture surfaces (K3, N3, and R3) had no significant difference in integral counts or detection-% compared to Piano MD 80 ground samples (K4, N4, and R4). However, it is important to note that if the fracture surface is very deep or otherwise pitted, the placement of the sample is important so that the X-rays can be detected (high enough take-off angle).

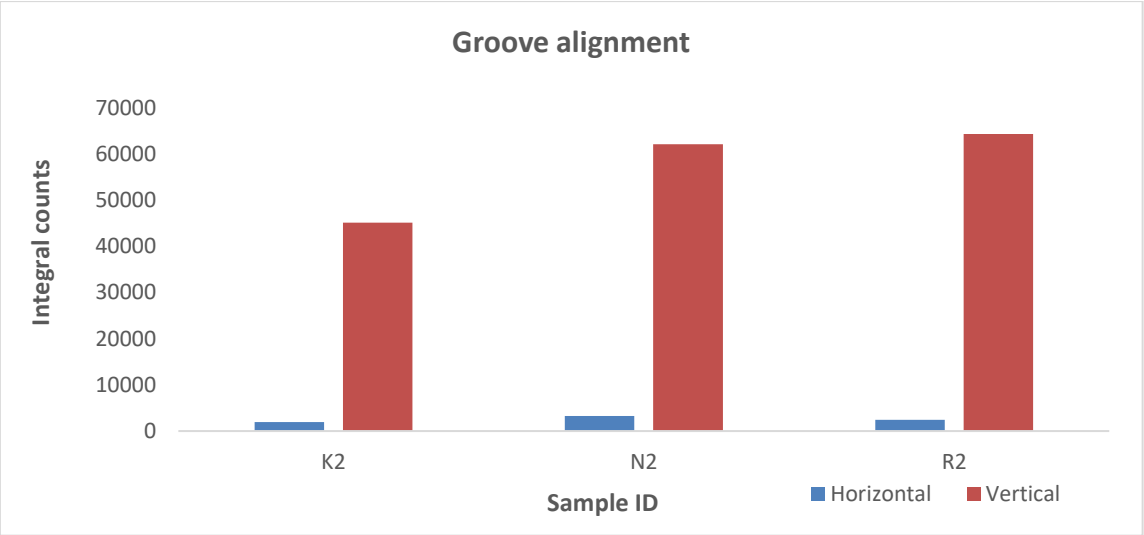

Figure 29. Graphical illustration of the importance of correct alignment when measuring samples containing grooves with an EDS detector. Blue columns indicate the integral counts when the groove is 90-degree angle to the detector and red columns show the integral counts when the groove is in-line with the detector. Integral counts decrease near zero if the groove is horizontally aligned.

The effect of corrosion was the last part of the surface quality analysis. After two weeks of rusting, both samples had a visible rusty surface. The fractured surface of sample A, which rusting process was accelerated with salt had dissolved pieces of material in a container. Figure 30 presents the samples after ultrasonic cleaning and drying. Even after the cleaning process, both samples had enough rusty surface to perform the surface quality analysis compared to the polished surface.

Figure 30. The left side marked with “A” illustrates the surface where the salt was added to increase the rusting process. The right side marked with “B” illustrates the corrosion propagation without additional salt. Both samples are washed with an ultrasonic cleaner.

Non-conductive impurities and oxides are visibly brighter areas in SEM images and affect negatively on the elemental analysis (Figure 31). The procedure was to select highly oxidized areas (bright area) and areas from the base material (dark area) to compare the possible differences in concentrations (Figure 31). The chemical composition results for both samples are presented in Table 14 and Table 15. As a result of 2 weeks of rusting, the most oxidized

measurement area contains 38,13 % oxygen (Table 15). Other impurities that result in their respective oxides through corrosion are natrium, nitrogen, chlorine, and calcium. The amount of all other elements in the standard is also highly affected by the rust.

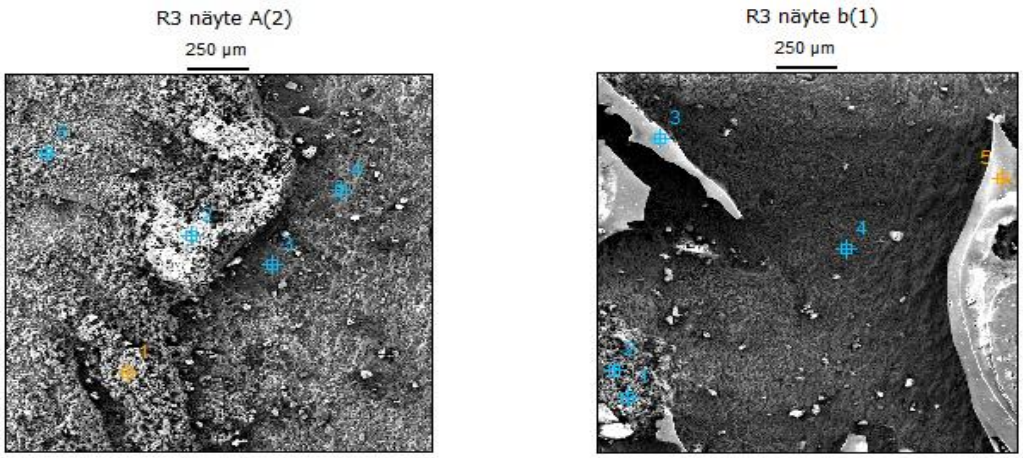

Figure 31. SEM images of the measurement areas for samples A and B. Bright areas are highly oxidized and darker areas (base material) have chemical composition closer to the standard values.

Chromium mass-% is at some points down to 0,17 %, which indicates that the rusting process has etched the protective chromium layer from the surface of the sample (Table 14 and 15). In sample A to which salt had been added, the corrosion had progressed deeper, and the values fluctuated considerably. In a few measurement areas, the integral counts remain low, which can be caused by the weak electrical conductivity of the thick oxide layer. Based on this measurement, it can be stated that rusty surfaces should always be polished if reliable elemental analysis is needed as the difference in chemical composition between the base material and the deeply rusted surface is significant.

Table 14. Chemical composition results of the sample A, highlighting the high oxidation, especially in measurement spots 1 and 3.

Elements	C	Cr	Fe	Mn	Mo	Ni	P	S	Si	O
Standard values (wt%)	0.30–0.38	1.30–1.70		0.50–0.80	0.15–0.30	1.30–1.70	≤ 0.025	≤ 0.035	≤ 0.40	-
Sample A / 1 (wt%)	0.56	0.17	60.49	0.18	0.05	0.24	0.00	0.15	0.32	**34.95**
Sample A / 2 (wt%)	0.00	0.24	93.35	0.12	0.35	0.40	0.02	0.00	0.03	4.55
Sample A / 3 (wt%)	0.48	10.96	60.35	0.93	0.47	2.41	0.06	0.15	0.57	**20.80**
Sample A / 4 (wt%)	0.00	14.37	70.87	3.18	0.0	1.58	0.00	0.12	0.02	9.11
Sample A / 5 (wt%)	0.00	3.75	88.62	1.16	0.06	1.06	0.00	0.00	0.11	4.50

Table 15. Chemical composition results of the sample B, highlighting the high oxidation, especially in measurements spots 1,2,3, and 5.

Elements	C	Cr	Fe	Mn	Mo	Ni	P	S	Si	O
Standard values (wt%)	0.30–0.38	1.30–1.70		0.50–0.80	0.15–0.30	1.30–1.70	≤ 0.025	≤ 0.035	≤ 0.40	-
Sample B / 1 (wt%)	0.44	0.28	66.11	0.16	0.00	0.35	0.04	0.03	0.33	**31.96**
Sample B / 2 (wt%)	0.42	0.32	69.55	0.22	0.00	0.60	0.02	0.03	0.40	**28.44**
Sample B / 3 (wt%)	0.45	0.17	60.26	0.16	0.05	0.17	0.02	0.01	0.19	**38.13**
Sample B / 4 (wt%)	0.43	4.17	80.97	0.87	0.24	1.16	0.02	0.01	0.32	11.18
Sample B / 5 (wt%)	0.40	0.19	65.13	0.25	0.06	0.39	0.01	0.00	0.15	**32.91**

6.3 Comparison between the devices

This section includes a comparison between the used research equipment in terms of accuracy and precision. The results presented in Figure 32 confirm that among the three devices under study, the OES is the most precise equipment for elemental analysis. This conclusion aligns with findings from previous component failure analyses performed in Wärtsilä Turku Investigation Laboratory and is further supported by the study of Zhang et al. [39]. The data presented in Figure 32 demonstrates the OES capability to consistently detect elements with low concentrations with low deviation (RSD ≤ 8), as indicated by the clustered data points in the bottom left corner.

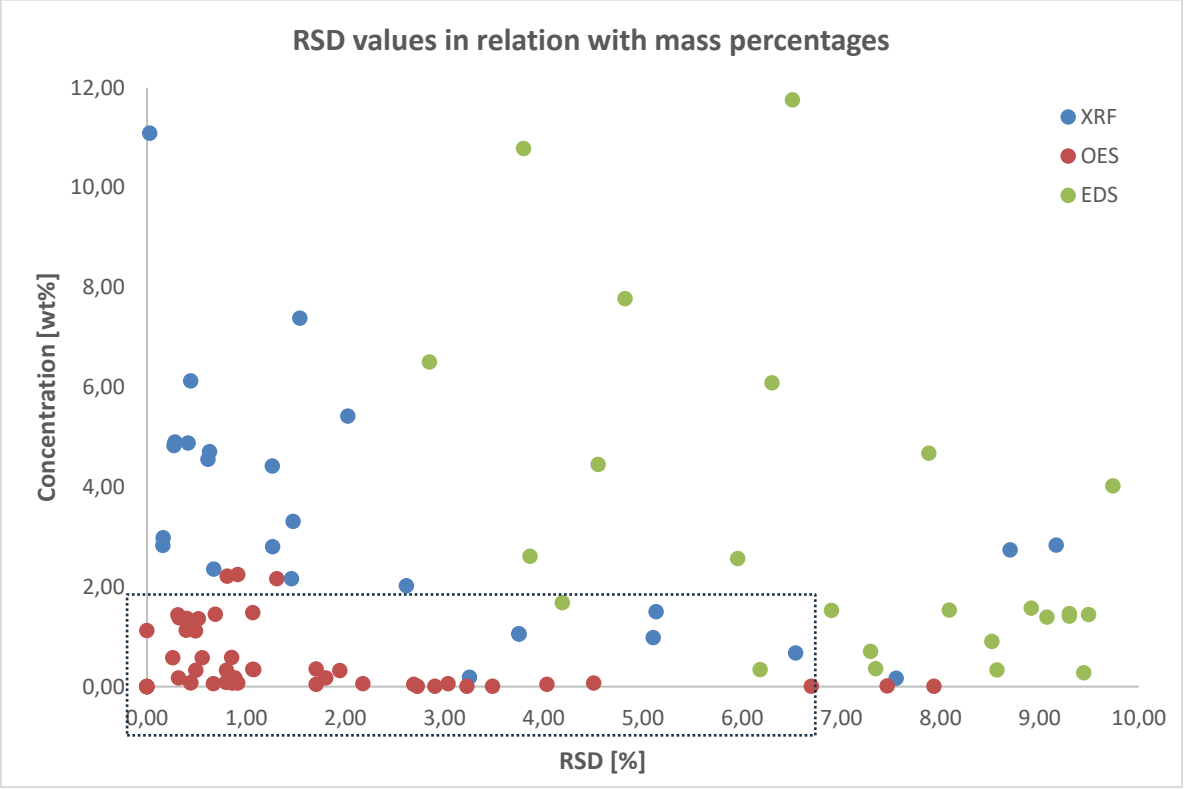

Figure 32. A comparative precision graph where the RSD values are presented in relation to wt%. Results from every measurement are included in this graph except K2, N2, and R2, since these are analyzed in surface quality section. Axels are intentionally limited as the focus is to illustrate precision of analytical techniques.

EDS initially shows only elements that it automatically identifies, and the rest need to be separately accessed from the periodic table according to the standard material composition. This analysis focuses mainly on those elements that have wt% over 0.1 as it is generally the limit of detection for EDS. Nickel was especially challenging for EDS to detect precisely as the RSD was constantly over 10. Lower concentration elements had very high RSD values (over 180) so it is not meaningful to present those here when the purpose is accuracy and precision.

The EDS method is suitable for analyzing small samples, drillings, grooves, and fractured or rusty surfaces. The green data points are more scattered around the graph but mainly focus on the bottom right corner (Figure 32). A clear trend with EDS (green spots) is noticed as the deviations decrease when concentrations increase. The results from samples K2, N2, and R2 are not included in Figure 32 as the groove and hole measurements are not meaningful to present this way. The graph is intentionally limited to RSD values that are below 10 %, as most of the points are in this scale and higher RSD means lower precision. Based on these results EDS cannot compete in accuracy and precision with OES when the purpose is to perform quantitative elemental analysis. EDS would be more suitable for qualitative analysis, where the goal is to determine the elements that are present.

The XRF analysis displays the largest variation, which can be seen by the scattered distribution of blue data points in Figure 32. Even low concentrations are detected reliably and most of the RSD values remain below 5. Major drawbacks occur with light elements as it is not capable of detecting for example carbon. However, the detection limit of XRF is better than EDS, which is further supported by the Nasrazadani et al. [13]. On the other hand, XRF is the only device in this study that can be used in hand-held mode which is important when investigating the chemical composition straight from the component before sample preparation.

In terms of light element detection, Figure 33 illustrates the atomic numbers from three studied materials in relation to RSD values to obtain the best device for light element detection. Results were similar to Figure 32 as the OES had the lowest RSD values even with light elements ($Z < 8$). XRF limitations are visible in this comparison as it detected no elements under atomic number 13 (aluminium). EDS detected more light elements than XRF, but the precision was moderate and the RSD values for carbon ($Z=6$) were from 7 to 15 % (Figure 33).

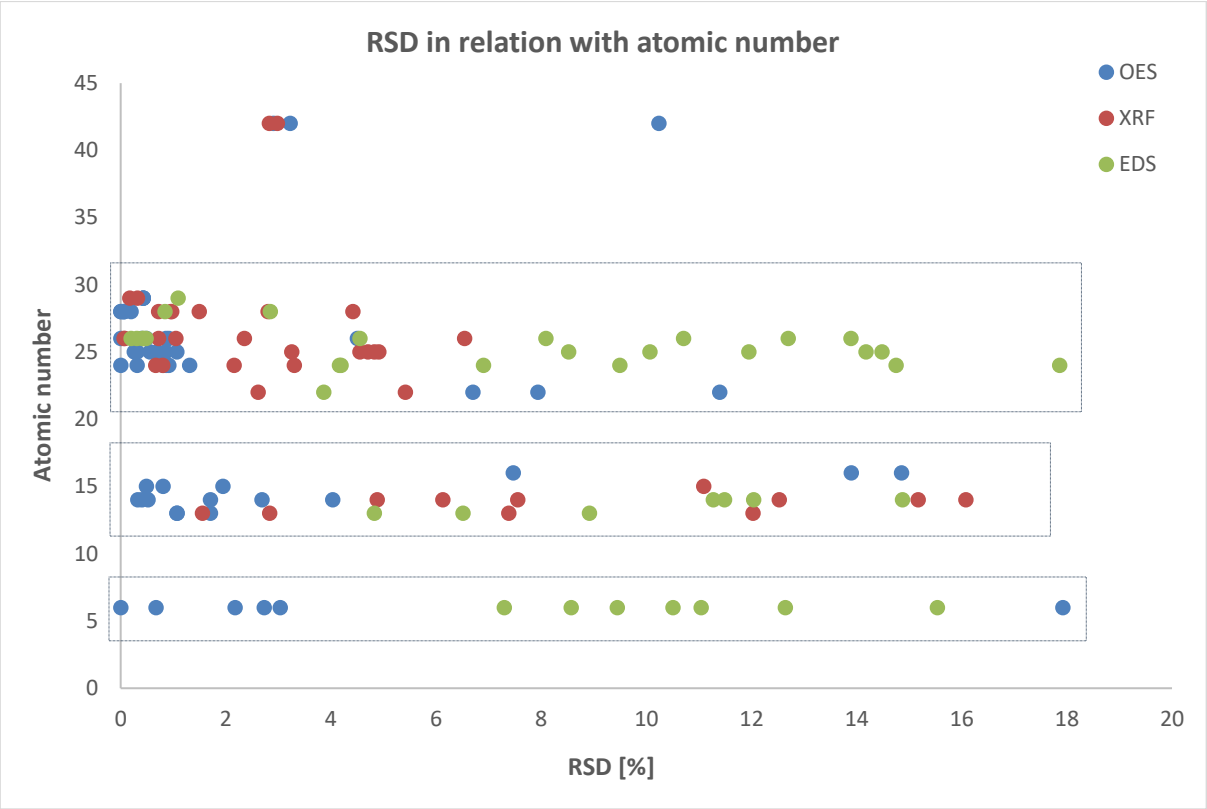

Figure 33. RSD values in relation to atomic numbers. OES results (blue points) are mainly focused on the left side of the graph which indicates high precision, even the lightest elements of the samples (carbon, aluminium, and silicon). XRF and EDS data points are more focused on the higher atomic number levels. However, the carbon (Z=6) was detected with 7-15 % precision (EDS).

Accuracy was another important parameter in this study, and it is presented for every analytical technique in Table 16. Match percentage means the number of values that match the standard values for certain materials. Detection-% means the percentage of detected elements compared to composition in material standard. Accuracy of XRF cannot meet the standard values for every element as the match percentage is around 50 % except for N1 and N4, which has a 100 % match percentage (Table 16). In addition, the detection-% is relatively low (around 50 %), except for R1 and R4 which have 77,8 %. This is mainly due to higher concentrations and a lower number of elements needing to be detected (only 9).

OES was also the most accurate device as the detection-% was almost 100 for both samples except for nickel alloy where the phosphorus was not detected. However, this can be considered a minor drawback as at the same time the match percentage was from 88,9 % up to 91,7 %. EDS results were more complicated to handle and interpret as there occurred overlapping (especially with Mo and S) which falsified the elemental results. Results are imported in the way as discussed in the EDS section which was to manually select all the standard elements for detection on the results table. There occurred some distortion as often the average value for

certain element was calculated only from one value which made it hit the standard. However, these are not the optimal values for EDS as the parameter optimization was done after this with a different setup.

Table 16. Accuracy comparison between the studied research devices in terms of detection-% and matching grade-%. Detection-% refers the percentage of the detected elements compared to standard. Matching grade-% describes the percentage of elements that has a chemical composition within the material standard values range.

Sample	Device	Elements in material standard	Detected elements	Detection %	Matching grade %
K1	XRF	12	6	50.0	50.00
K4		12	6	50.0	50.00
N1		13	7	53.8	100.00
N4		13	7	53.8	100.00
R1		9	7	77.8	57.14
R4		9	7	77.8	57.14
N4 RUN1	OES	13	12	92.3	91.67
N4 RUN2		13	12	92.3	91.67
N4 RUN3		13	12	92.3	91.67
R4 RUN1		9	9	100.0	88.89
R4 RUN2		9	9	100.0	88.89
R4 RUN3		9	9	100.0	88.89
K1	EDS	12	10	83.3	40.00
N1		13	12	92.3	75.00
R1		9	8	88.9	62.50
K3		12	11	91.7	63.64
N3		13	10	76.9	70.00
R3		9	8	88.9	62.50
K4		12	9	75.0	55.56
N4		13	11	84.6	90.91
R4		9	9	100.0	77.7

6.4 Further development ideas obtained from this study

The absence of a program and spark electrode for copper-alloy materials meant that the K4 sample could not be measured with OES. These tools would have improved the understanding of the composition of the copper sample, as it contained numerous elements in low

concentrations. The detection limits of XRF and EDS were not low enough to accurately detect these elements.

Sample preparation could be improved as the OES manufacturer has stated that the optimum roughness of the grinding wheel would be 60 when only 80 roughness was available for this study. On the other hand, the grinding could be done even with smaller particle sizes as Zhang et al used mesh number 40 in their study [39]. Further improvements for accuracy and precision would also be possible to achieve with a more frequent calibration interval.

As outlined in the OES results, the purity and concentration of Argon within the chamber are crucial for precise analysis. The Argon purity should be 99,998 % or higher and contain less than 5 ppm of O_2 and H_2O as the quality of analysis suffers when the Argon purity is 99,996 % or less. To address this, implementing a gas purification system between the OES and the Argon bottle could help mitigate potential fluctuations (Figure 34). Additionally, having an indicator to signal when the chamber is filled with Argon, displacing any air and particles, would greatly benefit the analysis process.

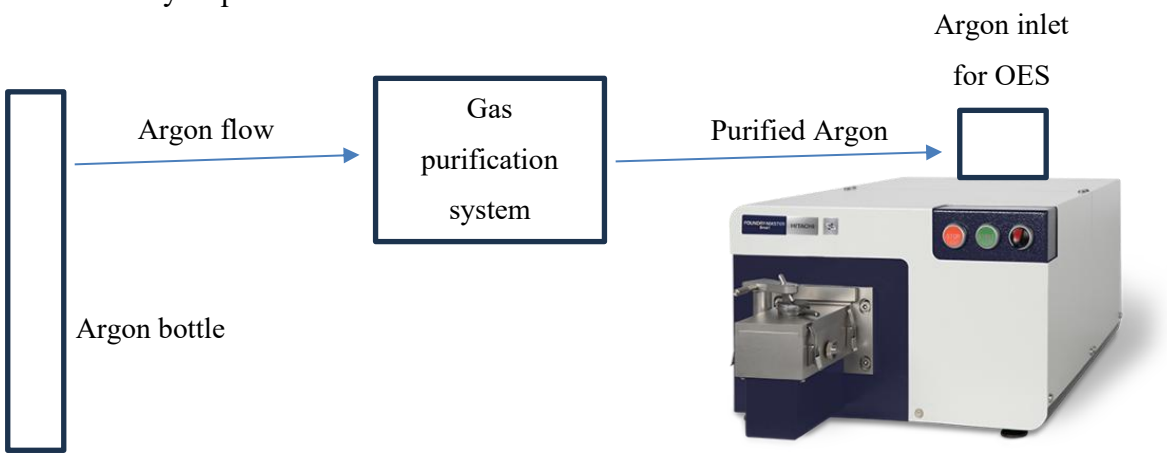

Figure 34. Schematic illustration of the possible gas purification system for OES.

6.5 Theory study results and analysis

This part of the thesis covers the results and analysis of the 2 theory questions presented in section 5.4. The first question was related to the harmfulness of wet/oily samples to SEM and the second was related to electromagnetic interference and its influences in SEM imaging.

6.5.1 Harmfulness of the wet/oily sample to SEM

Wet samples require extensive sample preparation, involving drying or freezing, followed by the coating or sectioning if imaged with conventional SEM. This makes the interpretation of

electron images of liquid systems more difficult because of the loss of volatile components and the possible introduction of artifacts [60]. An environmental scanning electron microscope (ESEM) is a more suitable technique for the study of the structure and dynamics of wet specimens as it is a capable method even for the study of fully liquid samples. It has some key advantages over SEM and requires no prior specimen preparation as it allows the presence of gas in the sample chamber [61].

Chamber vacuum causes evaporation when imaging wet specimens with SEM. This phenomenon can be mitigated by increasing chamber pressure, although, it can increase the temperature which accelerates the evaporation (Figure 35). The wet cover method, which was observed and studied by Inoue et al. is one option for imaging specimens that are sensitive to evaporation [62]. If there is low water vapor pressure the evaporation rate is high, and the specimen is no longer considered wet. Using a wet cover, the original surface water is retained and the specimen is still considered wet [62]. The wet cover method is graphically illustrated in Figure 36.

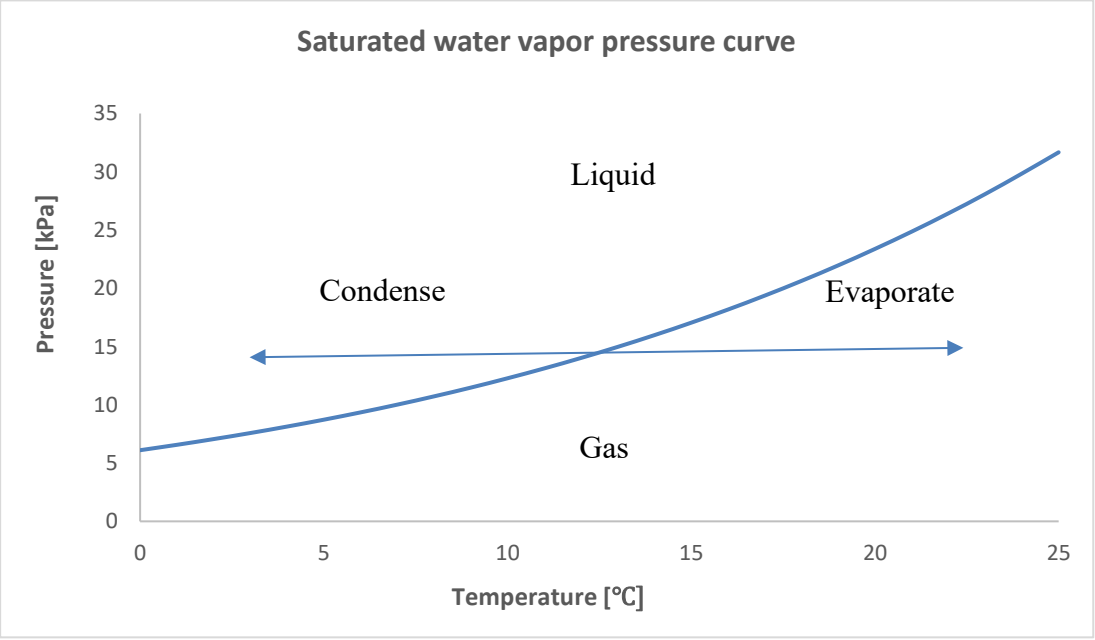

Figure 35. Saturated water vapor pressure curve

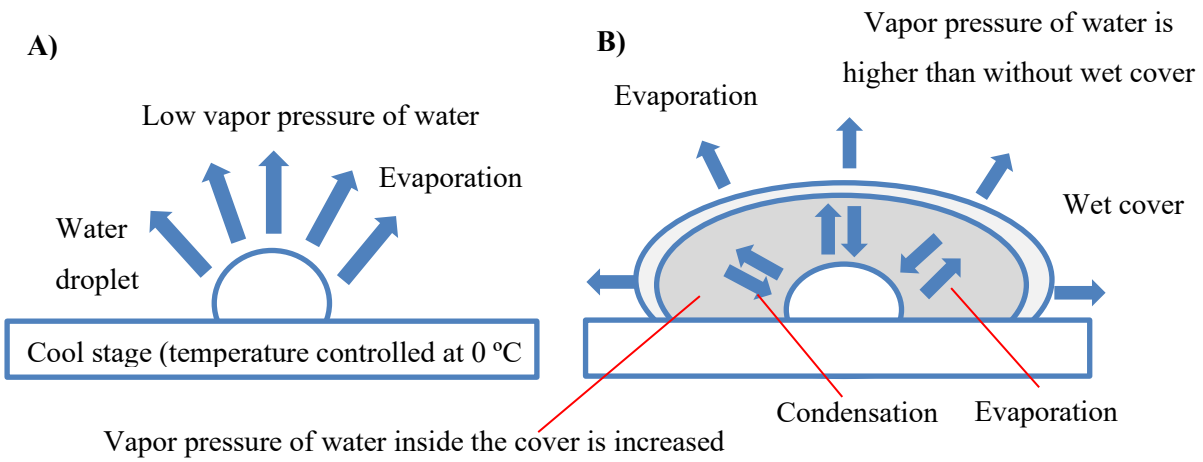

Figure 36. Wet cover method graphical illustration.

6.5.2 Electromagnetic interference sources and influences in SEM image

To obtain high-quality SEM images, it is essential to minimize environmental disturbances, including mechanical vibrations and electromagnetic interference. Electromagnetic interference (EMI) is one of the main sources of distortion in SEM image [63]. These distortions are usually visible as edge blur (low scan rate) or vibration (high scan rate) [64]. Vibration can be internal from SEM pumps or external, for example from construction or infrastructure work nearby. Image is highly affected by vibration if the magnification is more than 40 000 x (Figure 37).

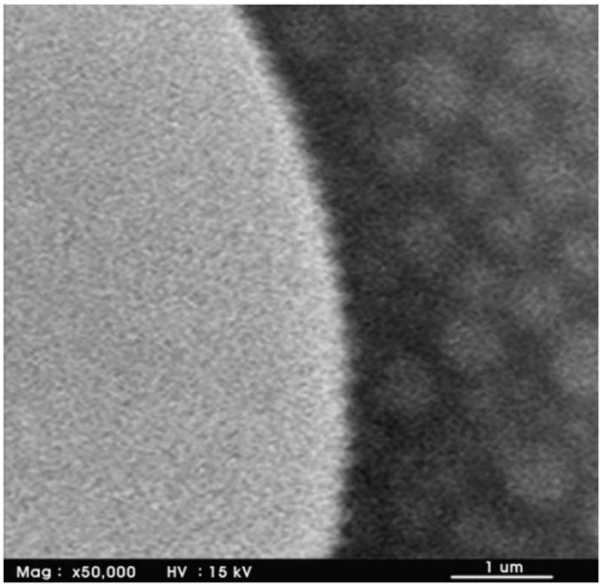

Figure 37. High magnification (40 000 x) SEM image introducing saw-toothed distortion on the edge of the specimen. Image reproduced with permission from [65]. Copyright 2012 Elsevier B.V.

The most common methods of electromagnetic interference reduction are electrostatic and magnetic shielding and/or active field compensation [64]. However, these hardware solutions are expensive and difficult to implement. To reduce these drawbacks Pluska et al. presented a method for differentiating various causes of SEM image distortions generated by EMI and relating the causes to specific elements of the SEM system to select optimal solutions for distortion reduction [63]. This method separates the direct influence of the magnetic field on the electron beam between the SEM final aperture and the above aperture [63]. Furthermore, it enables the measurement of the magnetic field present inside the SEM chamber [63].

7 Conclusion

In conclusion, this study aimed to determine the most suitable chemical analysis technique (XRF, SEM-EDS, OES) for various purposes and materials in terms of accuracy and precision. The study contained three different metal alloys (copper, nickel, iron) with four different samples and surface qualities (3 μm polished surface, cone and groove, fracture surface, and samples ground with mesh number 80) to obtain a wide comparative review. Furthermore, the goal was to investigate the root causes of carbon fluctuation in OES measurements. The research focused also on the optimal parameters to the extent that it was possible for each technique and included theory studies related to wet/oily specimen observation and electromagnetic interference with SEM.

After accuracy and precision measurements, OES was found to be the most accurate and precise equipment among the three studied devices. The carbon fluctuation needs to be considered either by deleting the first few results or intentionally flushing the chamber with Argon for a longer time. This eliminates the fluctuation (chamber is filled with Argon) and makes the analysis more reliable. XRF was found to be suitable for fast elemental analysis if the goal is to detect only the major elements of the material. It cannot detect carbon and other light elements so it cannot compete with OES. Based on this, XRF could be more useful in field investigations as OES is more powerful for elemental analysis in the laboratory.

SEM-EDS is most suitable for special shaped samples which include cones, grooves, or fracture surfaces. Analysis should be performed as qualitative as EDS cannot compete with OES in quantitative analysis as the detection limit is not low enough (0.10 wt%). The alignment of holes and grooves was found to have a significant effect, especially on the integral counts and the number of identified elements. This is due to low take-off angle which prevents the detection of X-rays. The most important operational parameters were found to be beam current and intensity (SEM) and dead time (EDS) which had the biggest impact on elemental analysis results. EDS elemental analysis the dead time should be 10-20 %, which means that beam intensity should be in a range of 15-17. In addition, false identifications due to spectral overlapping with Mo La and S Ka energy peaks caused false identifications which could be fixed with better spectral resolution (WDS).

References

[1] B. Akyuz and D. McKay, “Quantitative Chemical Analysis of Metals in Failure Analysis,” *J. Fail. Anal. Prev.*, vol. 22, no. 1, pp. 108–112, Feb. 2022, doi: 10.1007/s11668-021-01327-z.

[2] “3. Tools and Techniques - Knovel.” Accessed: Dec. 04, 2024. [Online]. Available: https://app-knovel-com.ezproxy.utu.fi/web/view/khtml/show.v/rcid:kpMFATCS01/cid:kt011PTYV3/viewerType:khtml/root_slug:metallurgical-failure/url_slug:tools-and-techniques?&b-toc-cid=kpMFATCS01&b-toc-root-slug=metallurgical-failure&b-toc-title=Metallurgical%20Failure%20Analysis%20-%20Techniques%20and%20Case%20Studies&b-toc-url-slug=introduction&kpromoter=federation&view=collapsed&zoom=1&page=2

[3] “Handbook of Materials Failure Analysis with Case Studies from the Oil and Gas Industry - 2.1.2 Scanning Electron Microscopy - Knovel.” Accessed: Nov. 26, 2024. [Online]. Available: https://app-knovel-com.ezproxy.utu.fi/web/view/pdf/show.v/rcid:kpHMFACSO1/cid:kt01102UB1/viewerType:pdf//root_slug:handbook-materials-failure/url_slug:modern-analytical-techniques?cid=kt01102UB1&b-toc-cid=kpHMFACSO1&b-toc-root-slug=handbook-materials-failure&b-toc-title=Handbook%20of%20Materials%20Failure%20Analysis%20with%20Case%20Studies%20from%20the%20Oil%20and%20Gas%20Industry&b-toc-url-slug=failure-analysis-oil&kpromoter=federation&view=collapsed&zoom=1&page=2

[4] “Is Scanning Electron Microscopy/Energy Dispersive X-ray Spectrometry (SEM/EDS) Quantitative?”, doi: 10.1002/sca.21041.

[5] G. Vukelić, G. Vizentin, G. Vukelić, and G. Vizentin, “Common Case Studies of Marine Structural Failures,” in *Failure Analysis and Prevention*, IntechOpen, 2017. doi: 10.5772/intechopen.72789.

[6] “Knovel - ASM Handbook, Volume 10 - Materials Characterization (2019 edition).” Accessed: Jan. 09, 2025. [Online]. Available: https://app.knovel.com/kn/resources/kpASMHVM2B/toc

[7] P. Seidel *et al.*, “Comparison of Elemental Analysis Techniques for the Characterization of Commercial Alloys,” *Metals*, vol. 11, no. 5, p. 736, 2021, doi: 10.3390/met11050736.

[8] E. Margui and R. Van Grieken, *X-ray Fluorescence Spectrometry and Related Techniques: An Introduction*. New York, UNITED STATES: Momentum Press, 2013. Accessed: Sep. 12, 2024. [Online]. Available: http://ebookcentral.proquest.com/lib/kutu/detail.action?docID=1048456

[9] Y. Leng, *Materials Characterization: Introduction to Microscopic and Spectroscopic Methods*. Newark, UNITED STATES: John Wiley & Sons, Incorporated, 2013. Accessed: Sep. 12, 2024. [Online]. Available: http://ebookcentral.proquest.com/lib/kutu/detail.action?docID=7104670

[10] “32. X-ray Spectroscopy - Knovel.” Accessed: Jan. 09, 2025. [Online]. Available: https://app.knovel.com/web/view/khtml/show.v/rcid:kpASMHVM2B/cid:kt012EILB1/viewerType:khtml//root_slug:32-X-ray-spectroscopy/url_slug:X-ray-spectroscopy?b-toc-cid=kpASMHVM2B&b-toc-title=ASM%20Handbook%2C%20Volume%2010%20-%20Materials%20Characterization%20%282019%20edition%29&b-toc-url-slug=X-ray-spectroscopy&view=collapsed&zoom=1.25&page=9

[11] “How does handheld XRF work? - FI.” Accessed: Aug. 06, 2024. [Online]. Available: https://www.thermofisher.com/uk/en/home/industrial/spectroscopy-elemental-isotope-analysis/spectroscopy-elemental-isotope-analysis-learning-center/elemental-analysis-information/xrf-technology.html

[12] A. A. S. Staff, “What is XRF (X-ray Fluorescence) and How Does it Work?,” Ask a Scientist. Accessed: Aug. 06, 2024. [Online]. Available: https://www.thermofisher.com/blog/ask-a-scientist/what-is-xrf-X-ray-fluorescence-and-how-does-it-work/

[13] S. Nasrazadani and S. Hassani, “Chapter 2 - Modern analytical techniques in failure analysis of aerospace, chemical, and oil and gas industries,” in *Handbook of Materials Failure Analysis with Case Studies from the Oil and Gas Industry*, A. S. H. Makhlouf and M. Aliofkhazraei, Eds., Butterworth-Heinemann, 2016, pp. 39–54. doi: 10.1016/B978-0-08-100117-2.00010-8.

[14] K. G. Mejía-Piña, M. A. Huerta-Diaz, and O. González-Yajimovich, “Calibration of handheld X-ray fluorescence (XRF) equipment for optimum determination of elemental concentrations in

sediment samples," *Talanta*, vol. 161, pp. 359–367, Dec. 2016, doi: 10.1016/j.talanta.2016.08.066.
[15] Measurlabs, "X-ray Fluorescence Spectroscopy | XRF Analysis Laboratory | Measurlabs." Accessed: Aug. 09, 2024. [Online]. Available: https://measurlabs.com/methods/X-ray-fluorescence-xrf/
[16] E. Pretorius, "Influence of acceleration voltage on scanning electron microscopy of human blood platelets," *Microsc. Res. Tech.*, vol. 73, no. 3, pp. 225–228, 2010, doi: 10.1002/jemt.20778.
[17] M. J. Yañez and S. E. Barbosa, "Changes in particle area measurements due to SEM accelerating voltage and magnification," *Microsc. Res. Tech.*, vol. 61, no. 5, pp. 463–468, 2003, doi: 10.1002/jemt.10309.
[18] "Intensity basics - EDS." Accessed: Nov. 21, 2024. [Online]. Available: https://myscope.training/EDS_Intensity_basics
[19] R. Flatabø, A. Coste, and M. m. Greve, "A systematic investigation of the charging effect in scanning electron microscopy for metal nanostructures on insulating substrates," *J. Microsc.*, vol. 265, no. 3, pp. 287–297, 2017, doi: 10.1111/jmi.12497.
[20] J. Cazaux, "Charging in scanning electron microscopy 'from inside and outside,'" *Scanning*, vol. 26, no. 4, pp. 181–203, 2004, doi: 10.1002/sca.4950260406.
[21] S. Maraghechi, J. P. M. Hoefnagels, R. H. J. Peerlings, O. Rokoš, and M. G. D. Geers, "Correction of Scanning Electron Microscope Imaging Artifacts in a Novel Digital Image Correlation Framework," *Exp. Mech.*, vol. 59, no. 4, pp. 489–516, Apr. 2019, doi: 10.1007/s11340-018-00469-w.
[22] O. C. Wells, "Scanning Electron Microscopy," in *Encyclopedia of Materials: Science and Technology*, K. H. J. Buschow, R. W. Cahn, M. C. Flemings, B. Ilschner, E. J. Kramer, S. Mahajan, and P. Veyssière, Eds., Oxford: Elsevier, 2001, pp. 8265–8269. doi: 10.1016/B0-08-043152-6/01479-0.
[23] J. I. Goldstein, D. E. Newbury, J. R. Michael, N. W. M. Ritchie, J. H. J. Scott, and D. C. Joy, "X-rays," in *Scanning Electron Microscopy and X-ray Microanalysis*, J. I. Goldstein, D. E. Newbury, J. R. Michael, N. W. M. Ritchie, J. H. J. Scott, and D. C. Joy, Eds., New York, NY: Springer, 2018, pp. 39–63. doi: 10.1007/978-1-4939-6676-9_4.
[24] R. W. Carpenter *et al.*, "• LAMET UFRGS • Ruth E. Whan Chairman Sandia National Laboratories".
[25] "Characteristic X-ray generation - EDS." Accessed: Sep. 18, 2024. [Online]. Available: https://myscope.training/EDS_Characteristic_X_ray_generation
[26] "Bremsstrahlung X-ray generation - EDS." Accessed: Nov. 20, 2024. [Online]. Available: https://myscope.training/EDS_Bremsstrahlung_X_ray_generation
[27] J. I. Goldstein, D. E. Newbury, J. R. Michael, N. W. M. Ritchie, J. H. J. Scott, and D. C. Joy, "Secondary Electrons," in *Scanning Electron Microscopy and X-ray Microanalysis*, J. I. Goldstein, D. E. Newbury, J. R. Michael, N. W. M. Ritchie, J. H. J. Scott, and D. C. Joy, Eds., New York, NY: Springer, 2018, pp. 29–37. doi: 10.1007/978-1-4939-6676-9_3.
[28] "Backscatter - SEM." Accessed: Nov. 22, 2024. [Online]. Available: https://myscope.training/SEM_Backscatter
[29] "What is energy dispersive spectroscopy? - EDS." Accessed: Jan. 09, 2025. [Online]. Available: https://myscope.training/EDS_What_is_energy_dispersive_spectroscopy
[30] M. f. Gazulla, M. Rodrigo, E. Blasco, and M. Orduña, "Nitrogen determination by SEM-EDS and elemental analysis," *X-ray Spectrom.*, vol. 42, no. 5, pp. 394–401, 2013, doi: 10.1002/xrs.2490.
[31] "What Dead Time you should choose for your EDS / EDX analysis?," Oxford Instruments. Accessed: Oct. 23, 2024. [Online]. Available: https://www.oxinst.com/blogs/what-dead-time-you-should-choose-for-your-eds-/-edx-analysis
[32] D. E. Newbury, "Mistakes encountered during automatic peak identification of minor and trace constituents in electron-excited energy dispersive X-ray microanalysis," *Scanning*, vol. 31, no. 3, pp. 91–101, 2009, doi: 10.1002/sca.20151.
[33] "EDS spectral resolution - EDS." Accessed: Sep. 19, 2024. [Online]. Available: https://myscope.training/EDS_EDS_spectral_resolution
[34] "TechFi™." Accessed: Nov. 13, 2024. [Online]. Available: https://micro.org.au/techniquefinder/Portal/viewTechnique/52

[35] "Energy Peak Overlapping in EDS Spectrum." Accessed: Nov. 20, 2024. [Online]. Available: https://www.globalsino.com/EM/page4634.html
[36] N. W. M. Ritchie, D. E. Newbury, and J. M. Davis, "EDS Measurements of X-ray Intensity at WDS Precision and Accuracy Using a Silicon Drift Detector," *Microsc. Microanal.*, vol. 18, no. 4, pp. 892–904, Aug. 2012, doi: 10.1017/S1431927612001109.
[37] "Optical Emission Spectroscopy Overview | OES | Hitachi High-Tech," Hitachi High Tech Analytical Science. Accessed: Oct. 07, 2024. [Online]. Available: https://hha.hitachi-hightech.com/en/blogs-events/blogs/2017/10/25/optical-emission-spectroscopy-(oes)/
[38] V. T. Services, "OES Electrode Cleaning | Tools, Tips & More," Verichek Technical Services. Accessed: Oct. 03, 2024. [Online]. Available: https://verichek.net/oes-electrode-cleaning.html
[39] Y. Zhang *et al.*, "Comparison of the Analytical Performances of Laser-Induced Breakdown Spectroscopy and Spark-OES," *ISIJ Int.*, vol. 54, no. 1, pp. 136–140, 2014, doi: 10.2355/isijinternational.54.136.
[40] "7. Optical Emission Spectroscopy - Knovel." Accessed: Jan. 09, 2025. [Online]. Available: https://app.knovel.com/web/view/khtml/show.v/rcid:kpASMHVM2B/cid:kt012EHZFA/viewerType:khtml//root_slug:7-optical-emission-spectroscopy/url_slug:asm-handbo-optical-emission?cid=kt012EHZG4&b-toc-cid=kpASMHVM2B&b-toc-title=ASM%20Handbook%2C%20Volume%2010%20-%20Materials%20Characterization%20%282019%20edition%29&b-toc-url-slug=asm-handbo-optical-emission&view=collapsed&zoom=1&page=1
[41] V. T. Services, "High-Purity Argon in OES Testing: Enhancing Accuracy & Reliability," Verichek Technical Services. Accessed: Dec. 16, 2024. [Online]. Available: https://verichek.net/high-purity-Argon-in-oes-testing.html
[42] D. A. Armbruster and T. Pry, "Limit of Blank, Limit of Detection and Limit of Quantitation," *Clin. Biochem. Rev.*, vol. 29, no. Suppl 1, p. S49, Aug. 2008.
[43] H.-K. Kim *et al.*, "Nanoscale light element identification using machine learning aided STEM-EDS," *Sci. Rep.*, vol. 10, no. 1, p. 13699, Aug. 2020, doi: 10.1038/s41598-020-70674-y.
[44] M. A. Khater, "Laser-induced breakdown spectroscopy for light elements detection in steel: State of the art," *Spectrochim. Acta Part B At. Spectrosc.*, vol. 81, pp. 1–10, Mar. 2013, doi: 10.1016/j.sab.2012.12.010.
[45] W. Admin, "Why light elements are difficult to measure with portable XRF," Portable Spectral Services. Accessed: Jan. 02, 2025. [Online]. Available: https://www.portaspecs.com/why-light-elements-are-difficult-to-measure-with-portable-xrf/
[46] T. Frost, "Quantitative Analysis," in *Encyclopedia of Spectroscopy and Spectrometry*, J. C. Lindon, Ed., Oxford: Elsevier, 1999, pp. 1931–1936. doi: 10.1006/rwsp.2000.0250.
[47] "Finding and Using Health Statistics." Accessed: Sep. 18, 2024. [Online]. Available: https://www.nlm.nih.gov/oet/ed/stats/02-900.html
[48] "Do you know how good your geochemical data is? APT does!," English. Accessed: Sep. 19, 2024. [Online]. Available: https://www.apt-int.com/news/do-you-know-how-good-your-geochemical-data-is-apt-does
[49] B. Davies, "Precision and accuracy in glacial geology," AntarcticGlaciers.org. Accessed: Sep. 04, 2024. [Online]. Available: https://www.antarcticglaciers.org/glacial-geology/dating-glacial-sediments-2/precision-and-accuracy-glacial-geology/
[50] A. M. Committee and A. No 56, "What causes most errors in chemical analysis?," *Anal. Methods*, vol. 5, no. 12, pp. 2914–2915, 2013, doi: 10.1039/C3AY90035E.
[51] G. V. Hartland, "Statistical Analysis of Physical Chemistry Data: Errors Are Not Mistakes," *J. Phys. Chem. A*, vol. 124, no. 11, pp. 2109–2112, Mar. 2020, doi: 10.1021/acs.jpca.0c01403.
[52] "4. Systematic vs. Random Errors | The Nature of Geographic Information." Accessed: Nov. 01, 2024. [Online]. Available: https://www.e-education.psu.edu/natureofgeoinfo/c5_p5.html
[53] A. Banerjee, U. B. Chitnis, S. L. Jadhav, J. S. Bhawalkar, and S. Chaudhury, "Hypothesis testing, type I and type II errors," *Ind. Psychiatry J.*, vol. 18, no. 2, pp. 127–131, 2009, doi: 10.4103/0972-6748.62274.
[54] "Equipment | INSTITUTE FOR METALS SUPERPLASTICITY PROBLEMS OF THE RUSSIAN ACADEMY OF SCIENCES." Accessed: Oct. 22, 2024. [Online]. Available: https://www.imsp.ru/en/node/373

[55] "DELTA Premium | Olympus IMS." Accessed: Oct. 22, 2024. [Online]. Available: https://www.olympus-ims.com/en/delta-premium/#!cms[focus]=cmsContent11677
[56] "Stationary OES | Optical Emission Spectrometer | Hitachi High-Tech," Hitachi High Tech Analytical Science. Accessed: Aug. 09, 2024. [Online]. Available: https://hha.hitachi-hightech.com/en/product-range/products/optical-emission-spectrometers/stationary-spark-spectrometers-oes
[57] "Total Materia :: Chemical Composition." Accessed: Nov. 07, 2024. [Online]. Available: https://portal.totalmateria.com/en/search/quick/materials/3040346/composition
[58] "Total Materia :: Chemical Composition." Accessed: Nov. 07, 2024. [Online]. Available: https://portal.totalmateria.com/en/search/quick/materials/3290965/composition
[59] "Total Materia :: Chemical Composition." Accessed: Nov. 07, 2024. [Online]. Available: https://portal.totalmateria.com/en/search/quick/materials/1050135/composition
[60] R. G. Mathews and A. M. Donald, "Conditions for imaging emulsions in the environmental scanning electron microscope," *Scanning*, vol. 24, no. 2, pp. 75–85, 2002, doi: 10.1002/sca.4950240205.
[61] A. M. Donald, "Environmental scanning electron microscopy for the study of 'wet' systems," *Curr. Opin. Colloid Interface Sci.*, vol. 3, no. 2, pp. 143–147, Apr. 1998, doi: 10.1016/S1359-0294(98)80006-X.
[62] N. Inoue, Y. Takashima, M. Suga, T. Suzuki, Y. Nemoto, and O. Takai, "Observation of wet specimens sensitive to evaporation using scanning electron microscopy," *Microscopy*, vol. 67, no. 6, pp. 356–366, Dec. 2018, doi: 10.1093/jmicro/dfy041.
[63] M. Płuska, A. Czerwinski, J. Ratajczak, J. Kątcki, Ł. Oskwarek, and R. Rak, "Separation of image-distortion sources and magnetic-field measurement in scanning electron microscope (SEM)," *Micron*, vol. 40, no. 1, pp. 46–50, Jan. 2009, doi: 10.1016/j.micron.2008.01.009.
[64] M. Płuska, A. Czerwinski, J. Ratajczak, J. Kątcki, and R. Rak, "Elimination of scanning electron microscopy image periodic distortions with digital signal-processing methods," *J. Microsc.*, vol. 224, no. 1, pp. 89–92, 2006, doi: 10.1111/j.1365-2818.2006.01672.x.
[65] K. O. Jung, S. J. Kim, and D. H. Kim, "An approach to reducing the distortion caused by vibration in scanning electron microscope images," *Nucl. Instrum. Methods Phys. Res. Sect. Accel. Spectrometers Detect. Assoc. Equip.*, vol. 676, pp. 5–17, Jun. 2012, doi: 10.1016/j.nima.2012.01.061.